

Vulnerability to cavitation and response of canopy conductance to root cavitation in five
southeastern US pine species

By

Student: Haoyu Zhang

Advisors: Dr. Jean-Christophe Domec and Dr. Ram Oren

December 8, 2021

Masters project submitted in partial fulfillment of the
requirements for the Master of Forestry and the Master of Environmental Management
concurrent degree in
The Nicholas School of the Environment of
Duke University

Abstract

Although the Southeastern United States generally receives considerable precipitation and total precipitation has slightly increased, the region has experienced recent recurrent droughts and is anticipated to encounter more severe droughts as a result of increasing temperature (National Integrated Drought Information System). Knowledge of plant water transport and plant organ hydraulics facilitates our understanding of the capabilities of forests to withstand drought under a changing climate.

In this project, we studied five pine species that are ecologically or economically important in the Southeastern US, namely *Pinus virginiana* (Virginia pine), *P. echinata* (shortleaf pine), *P. taeda* (loblolly pine), *P. elliottii* (slash pine), and *P. palustris* (longleaf pine). The overarching goal is to understand and compare their hydraulic performance under droughts. We addressed the goal from two perspectives. First, we compared hydraulic properties associated with vulnerability to embolism curves for terminal branches and lateral roots in the topsoil. The properties analyzed included the water potential at which 50% xylem specific conductivity is lost (P_{50}), and the slope of the vulnerability curve at P_{50} (S_{50}), saturated xylem specific conductivity (k_{sat}), and leaf specific conductivity (LSC), a proxy for a given area of wood (xylem) to supply water to the leaves.. We employed a Bayesian hierarchical model modified from a previous study to estimate the hydraulic parameters for the two organs of each species. The efficiency-safety tradeoff was tested at sample level in branches and roots.

The second perspective was to investigate the stomatal regulation strategies adopted by these species. For this purpose, we studied the response of canopy conductance index (G_cJ) to the estimated *in situ* loss of conductivity in roots (PLC_{root}) during the growing season of 2019. There has been established knowledge about the response of canopy conductance to air vapor pressure deficit (VPD). Thus, we explored how variation in G_cJ that was unexplained by VPD could be explained by PLC_{root} , and compared the response of G_cJ to PLC_{root} across species. Two methods of estimating soil water potential, from which PLC_{root} was computed, were used by either assuming random noise in measurements on soil texture or assuming representation of microsite variability by the measurements. The response of G_cJ to PLC_{root} was analyzed with the two methods to study how the two underlying assumptions about microsite variability in soil texture might affect results and interpretation on the response.

We found that among all the species, resistance to cavitation was similar in branches but appeared to have an increasing trend in roots from shorter- to longer-needle species. In contrast, k_{sat} was similar in roots, but was highest in the two provenances of *P. taeda* and appeared to be slightly lower in shorter-needle species. Despite the similarity in k_{sat} in branches, LSC appeared to have an increasing trend from longer- to shorter-needle species, except for the short-needle *P. echinata* that also had low LSC. We did not find strong evidence for a negative correlation between P_{50} and k_{sat} at sample level in branches and

roots, as suggested by the efficiency-safety tradeoff. However, roots were slightly more likely to exhibit such a tradeoff than branches were.

If the assumption about random noise in soil texture was taken, the sensitivity of G_cJ unexplained by VPD to cavitation in roots was similar in the studied species, except for *P. elliottii*, which was distinctly insensitive compared to the others. When comparing at the same level of cavitation in roots, *P. virginiana*, *P. echinata*, and one of two genotypes of *P. taeda* (PT1) were likely to have lower G_cJ than the others. However, *P. taeda* PT1 was expected to experience greater extent of cavitation in roots than *P. virginiana* and *P. echinata* due to their difference in resistance to cavitation. With the assumption about representing microsite variability, both sensitivity of G_cJ and G_cI at the same level of root cavitation showed greater difference among species. Despite the different method employed, *P. elliottii* still remained the most insensitive species, while *P. echinata* and *P. taeda* (PT2) were the most sensitive and had lower canopy conductance than the others when comparing at the same level of root cavitation.

Overall, the results suggest that the two short-needle species, *P. virginiana* and *P. echinata*, are likely to be more resistant to drought by the combined benefit of higher resistance to cavitation in roots and moderate to conservative regulation of G_cJ . The study also calls attention to the assumption made for microsite variability in soil texture, when using common garden to study relationships among functions of different organs that entail soil water conditions.

Table of Contents

| | |
|--|----|
| Introduction..... | 5 |
| Methods | 8 |
| Plant Materials | 8 |
| Fitting Vulnerability Curves | 9 |
| Frequentist Approach..... | 10 |
| Bayesian Approach | 10 |
| Daily Canopy Conductance Index | 13 |
| Estimating In Situ Root PLC | 14 |
| Soil Water Content..... | 14 |
| Soil Water Potential | 14 |
| Response of Canopy Conductance Index to Root Cavitation | 15 |
| Results..... | 16 |
| Vulnerability Curves..... | 16 |
| Environmental Water Conditions and Daily Canopy Conductance Index..... | 19 |
| Response of Canopy Conductance Index to Root Cavitation | 22 |
| Discussion..... | 25 |
| Hydraulic Parameters..... | 25 |
| Soil Water Conditions and Response of Canopy Conductance Index to Root Cavitation..... | 26 |
| Acknowledgement | 28 |
| References..... | 29 |
| Supplementary Materials | 32 |

Introduction

Water loss from leaves through stomata (i.e. transpiration) occurs concurrently with the diffusion of carbon dioxide (CO_2) from the atmosphere into leaf intercellular airspace, where CO_2 enters mesophyll and is assimilated in chloroplasts. The transpired water is replenished by the water that is extracted from the soil at roots and then transported via xylem to leaves, forming the soil-plant-atmosphere continuum (SPAC).

Stomata is the primary site regulating transpiration and consequently whole-plant water status. At high water availability, stomata will be near complete open state to maximize CO_2 uptake for photosynthesis, but gradually decrease aperture and thus g_s with the progress of water deficit. Stomatal conductance (g_s) declines with the natural logarithm of water pressure deficit (VPD) at a fairly constant rate; transpiration increases with VPD almost linearly when VPD is low, but reaches a plateau and starts to decline at high VPD as g_s decreases (Oren *et al.*, 1999). Numerous models, both empirical and mechanistic have been proposed to describe g_s as a function of environmental factors (e.g. VPD, water potential), related physiological processes (e.g. photosynthesis, transpiration), or internal molecular cue(s) (e.g. abscisic acid) (Damour *et al.*, 2010). Despite the different approaches to understanding the mechanisms underlying stomatal regulation, there is a continuum of regulation strategy of minimum leaf water potential between two extremes – isohydricity, which maintains leaf water potential and prevents it from dropping under water stress, versus anisohydricity, which does not maintain leaf water potential around a fixed value but instead allows leaf water potential to decline with drought severity (Woodruff *et al.*, 2016; Grossiord *et al.*, 2020). More investigation is necessary to quantify stomatal regulation differences across functional groups, and how other traits are coordinated with stomatal sensitivity (Grossiord *et al.*, 2020).

Along SPAC, water is elevated by the combined effect of the tension generated as water evaporating at capillary menisci and the cohesion between water molecules (Dixon, 1914; Vilagrosa *et al.*, 2012). The consequence of this tension-cohesion effect is that during transpiration xylem experiences negative water potential (i.e. negative pressure). In plants, water potential (Ψ) stays well below the saturated vapor pressure of water, which is 2.3 kPa at 20°C and -99 kPa at sea level, and therefore xylem sap is in a metastable state relative to the gas phase with lower energy (Tyree & Sperry, 1989; Lens *et al.*, 2013). In order to maintain the continuity of water column, nucleation of vaporization (i.e. cavitation) and consequently the state of being vapor-filled in plant conduits (i.e. embolism) must be prevented (Tyree & Sperry, 1989). If the water column is broken and embolism occurs, the ability of xylem to transport water is greatly reduced (Lens *et al.*, 2013).

There are three major causes under natural settings for embolism: drought, frost, and pathogens (Tyree & Sperry, 1989). Two hypotheses have been proposed for the mechanism of drought-induced embolism. The first one is homogenous nucleation in which water vapor forms spontaneous in bulk water, but this

process requires extremely negative pressure that cannot be found in plants (from -30 to -140 MPa) (Lens *et al.*, 2013). The other is heterogenous nucleation, or air-seeding theory which holds that air bubbles (emboli) form at the interface between water and pit membrane or cell wall when air is aspirated into water-filled conduits from neighboring embolized conduits due to abscission, breakage, damage, or normal development in ruptured protoxylem strands (Lens *et al.*, 2013). With progressively negative pressure, these air bubbles enlarge and propagate from conduits to conduits, further decreasing xylem conductivity. In frost-induced embolism, bubbles develop because of the insolubility of air in ice, and on thawing may expand under negative pressure (Tyree & Sperry, 1989; Mayr & Sperry, 2010). Finally, pathogens can induce embolism either through occlusion of pathogenic materials or indirectly through interaction with water stress (Vilagrosa *et al.*, 2012).

Xylem vulnerability to embolism can be quantitatively examined with vulnerability curve (VC), in which percentage loss of conductivity (PLC) representing the extent of embolism is plotted against water potential. Different mathematical and statistical models have been proposed to fit VC, and the two most commonly used are sigmoidal (Pammenter & Van Der Willigen, 1998) and Weibull (Neufeld *et al.*, 1992). With interpolations from these models, indices have been devised to quantify vulnerability (P_{12} , P_{50} , P_{88}), of which the most commonly used is P_{50} (also termed Ψ_{50}), the water potential at which 50% of xylem specific conductivity (k_s) is lost (Domec & Gartner, 2001). The sensitivity (S_{50}) to decline in water potential represented by the slope of PLC at a particular water potential (e.g. at P_{50}) is another parameter derived from VC, and reflects how rapid embolism develops with increasing tension. However, this index has been computed less often than the water potential required for a certain degree of embolism, such as P_{50} (Ogle *et al.*, 2009). This contrasts with the great attention paid to species and condition differences in the sensitivity of g_s to changing vapor pressure deficit. Presumably one obstacle to comparing S_{50} in xylem among species and conditions is the difficulty in extracting S_{50} from the curves. In fact, only sigmoid function has parameters inherently reflecting both P_{50} and S_{50} (Ogle *et al.*, 2009). To address the issue, Ogle *et al.* (2009) proposed a Bayesian hierarchical model that uses reparameterized sigmoidal and Weibull equations that are expressed in terms of biologically interpretable vulnerability and sensitivity parameters instead of the original mathematical parameters.

Another widely discussed topic regarding xylem transport is the efficiency-safety tradeoff theory. It has long been assumed to be a universal principle that applies to most of vascular plants. “Efficiency” refers to k_s , while “safety” refers to the xylem vulnerability, such as P_{50} (Gleason *et al.*, 2016). The theory posits that xylem functionality is determined by pits and xylem network in such a way that increase in one aspect of efficiency or safety causes decline in maximum capacity of the other (Gleason *et al.*, 2016). Many mechanisms are thought to be involved in this negative linkage. For example, wider xylem conduits

tend to have greater pit membrane area per vessel and more large pores which allows air-seeding of cavitation to occur at a higher water potential (Wheeler *et al.*, 2005).

The tradeoff theory has been well tested and supported by comparison among relatively closely related groups (e.g. Domec & Gartner, 2001; Martínez-Vilalta *et al.*, 2002; Hacke *et al.*, 2006; Lens *et al.*, 2011). However, an evolutionary basis for the tradeoff was not supported by phylogenetically independent contrast correlation, which includes phylogenetic information and accounts for similarity between related species when comparing traits (Maherali *et al.*, 2004). Gleason *et al.* (2016) examined an extensive range of species using TRY database and found that not all species lie in the hypothesized zone extending from top left to bottom right on an efficiency vs. safety diagram (cf. Fig. 1 in their article). Although no species was found to have both high efficiency and high safety, some species fall into the region representing low efficiency and low safety. The presence of low-efficiency low-safety category suggests that unrealized traits may confound our understanding on the relationship between the two aspects (Gleason *et al.*, 2016). Efficiency is dictated by many xylem properties, such as conduit lumen fraction, ultrastructure of pits, connectivity of conduit network, and Gleason *et al.* (2016) argued that not all improvements in efficiency by these mechanisms would reduce safety.

McCulloh *et al.* (2019) and Grossiord *et al.* (2020) pointed out that studies on plant organ-level response to water stress are undoubtedly valuable in advancing our knowledge on plant hydraulics, but it is also necessary not to forget to take an holistic perspective on these hydraulic traits together with others, from whole-plant to ecosystem and landscape levels, to better understand how plants will perform in a world with continuously growing water deficit.

In the present study, we fitted vulnerability curves for both terminal branches and surface roots in five common pine species (*Pinus virginiana*, *P. echinata*, *P. taeda*, *P. elliottii*, *P. palustris*) in Southern US and compared hydraulic parameters relevant to the curves, namely P_{50} , S_{50} , saturated xylem specific conductivity (k_{sat}), and leaf specific conductivity (LSC). Efficiency-safety hypothesis was tested between P_{50} and k_{sat} in branches and roots, respectively. To explore how different compartments of whole trees are coordinated under changing water conditions in the field, we predicted *in situ* root PLC during the growing season in 2019 (April 1 to November 12) based on the fitted vulnerability curves and examined the response of canopy conductance, using a surrogate daily index, to *in situ* root PLC after accounting for the effect of VPD on canopy conductance.

Methods

Plant Materials

We studied five pine species (*P. virginiana*, *P. echinata*, *P. taeda*, *P. elliottii*, *P. palustris*) including two *P. taeda* variants with narrow (PT1) or broad (PT2) crown shape that were growing in an experimental plantation in Duke Forest, Durham, NC, US ($36^{\circ}01' N$, $78^{\circ}59' W$). One-year-old seedlings of all the species were planted in 2011 in 32×40 m plots at 4×2 m spacing. In the present study, the two variants were treated as two species groups, leading to a total of six species groups considered in all subsequent analyses. Because *P. palustris* trees were too small to accommodate thermal dissipation probes and sampling in 2019, trees in a nearby plot planted a year earlier were used instead. On average the site had Appling sandy loam, mean annual temperature of $15.5^{\circ}C$, and annual precipitation of 1145 mm evenly distributed throughout the year.

Branch samples were collected by excising 50-60 cm of branch from the tip in the middle to upper crowns, and then another 15-20 cm of short branch segment was excised from the cut end. All the needles were removed and stored in a plastic bag, while the short branch segments were soaked into water to prevent unintended embolism during transportation. Root segments with a length of 11-18 mm and a diameter of 6-15 mm were excised from lateral roots in topsoil. In order to prevent air being aspirated into xylem by tension during excision, the proximal end of the root segments was first cut, and then the distal end. All root segments were also stored in water. We collected one branch and one root samples from six trees per species, leading to a total of 72 samples.

In the laboratory, branch and root segments were soaked in water in a container that is connected to a vacuum outlet for at least 24 h to suction any cavitation out of the xylem. Then the pressure sleeve method (also known as air injection, air pressurization) (Cochard *et al.*, 2013; Martin-Stpaull *et al.*, 2014), was used to introduce cavitation at 0, 0.5, 2, 4, 5, 6, 7 MPa for branch samples and at 0, 0.5, 1, 2, 3, 4, 5 MPa for root samples. For samples that lost nearly all of conductivity before the highest intended pressure was employed, lower pressure was employed as final.

For branch samples, total leaf area (A_L) of the needles supplied by each segment was estimated from measured total dry mass of the needles divided by the leaf mass per area (LMA), obtained from Wang *et al.* (2019) who quantified LMA on the same species and experimental site. The needles supplied by the segment is defined as all the needles growing on the long branch sample connected to the segment, plus half of the needles of the segment.

To calculate safety margin, leaf water potential (LWP) was measured at predawn and midday of a day during the dry season in 2017, 2018, and 2019. LWPs measured in 2017 were the most negative for all species and thus selected as the observed minimum values. Given that the saplings were not tall (<3m), observed minimum water potentials in roots were assumed to equal LWPs at predawn when transpiration

was zero. LWPs at midday was used as the observed minimum water potentials in branches. Safety margin was calculated as observed minimum water potential in each organ minus P_{50} of the organ. For P_{50} estimated by Bayesian approach, posterior draws were directly subtracted from species average for each organ (i.e. a constant), and posterior means and credible intervals for safety margins were computed accordingly.

Fitting Vulnerability Curves

To fit vulnerability curves (VCs), xylem specific conductivity (k_s) in $\text{kg m}^{-1} \text{s}^{-1} \text{MPa}^{-1}$ was first calculated following Darcy's law:

$$k_s = \frac{QL}{\Delta PA_s} \quad (1)$$

where Q is flow rate of water in kg s^{-1} measured by the pressure sleeve method, L is sample length, ΔP is the difference in pressure in MPa between two ends of sample and in the present study was the pressure exerted by the waterhead (constant at 0.0047 MPa), A_s is sapwood area in m^2 and here was calculated as the mean of the sapwood areas at two ends. Then relative conductivity ($relK$) and percent loss of conductivity (PLC), which are complementary to each other, were calculated:

$$relK = \frac{k_s}{k_{sat}} = 1 - \frac{PLC}{100\%} \quad (2)$$

Where k_s is conductivity at a given pressure level, and k_{sat} is saturated conductivity when no cavitation occurs. Sigmoid (Pammenter & Van Der Willigen, 1998) and Weibull (Neufeld *et al.*, 1992) are the two most commonly used functional forms to fit VCs. In the present study, Weibull was used because it ensures $relK = 1$ when $P = 0$, and the reparameterized form by Ogle *et al.* (2009) was selected so that the function is expressed in terms of physiological meaningful parameters (Eq 3).

$$k_s = k_{sat} \cdot relK = k_{sat} \left(1 - \frac{X}{100} \right)^{\left[\left(\frac{P}{P_X} \right)^{\frac{P_X S_X}{V}} \right]} \quad (3)$$

$$V = (X - 100) \ln \left(1 - \frac{X}{100} \right)$$

where k_s is predicted conductivity at pressure P , k_{sat} is saturated conductivity, P is positive-valued water potential (i.e. pressure applied) in MPa, P_X is positive-valued water potential at which X% of conductivity is lost, S_X is the slope of VC at P_X in $\% \text{ MPa}^{-1}$. Fifty (i.e. P_{50} and S_{50}) is most frequently discussed in literature, so X was fixed at 50 in the present project, and V was a constant.

Given k_{sat} , LSC is calculated as follows:

$$LSC = k_{sat} \cdot \frac{A_s}{A_L}$$

where A_s is sapwood area of a branch segment, and A_L is total leaf area supplied by a branch segment. For convenience, LSC was expressed in $10^{-4} \text{ kg m}^{-1} \text{ s}^{-1} \text{ MPa}^{-1}$.

Frequentist Approach

The package “fitplc” (Duursma & Choat, 2017) that estimates parameters by nonlinear least squares was used to fit VC for each sample, and the maximum k_s observed for each sample was regarded as its saturated k_s . We performed one-way ANOVA to estimate species effect on the PLC parameters (P_x, S_x) for branch and root respectively, and confidence intervals were *post hoc* adjusted by multivariate *t*-distribution for multiplicity using “emmeans” package.

Bayesian Approach

The hierarchical nature of the data with multiple levels, from species, trees, organs (branch vs root), measurements on the same segment at different pressures, indicates that a Bayesian hierarchical (BH) model can be used to fit VC and the hydraulic parameters derived from it. Also of interest is the quantifiable uncertainty in the parameters that can be directly estimated by one model. The BH model used here was mostly adopted from Ogle *et al.* (2009) with some modifications. First, k_{sat} was fitted on its original instead of relative value so that estimates for k_{sat} are directly comparable across species. Second, Ogle *et al.* used univariate normal for each of the three hydraulic parameters (P_{50}, S_{50}, k_{sat}), and here we used multivariate normal so that the efficiency-safety hypothesis can be evaluated at individual level for branch and root respectively, using the correlation matrix derived from the covariance matrix in multivariate normal. Third, we also measured A_L supplied by each branch sample and thus added LSC that was based on k_{sat} and data on A_L . Fourth, because only one sample per organ was taken from each tree, random effect at tree level proposed in the work by Ogle *et al* cannot be estimated and was omitted in the present study. Fifth, in the present study hydraulic parameters had variance depending on organ type instead of a common variance between branch and root. Finally, Ogle *et al.* included an unknown parameter for the initial water potentials after flushing the segment, while in the present study samples were soaked in water under negative pressure to remove native cavitation, so the first measurement without pressure was assumed to be taken at $P = 0$. Priors for parameters were also different.

The BH model consists of three stages: 1) data model, 2) process model, and 3) parameter model (Clark, 2004).

Stage 1 Data model. For measurement n on sample i of organ t and species s , relative conductivity $relK$ is distributed as follows:

$$K \sim N(\mu_{\{n,i,t,s\}}, \sigma_y^2) \quad (4)$$

where K is the ratio of measured k_s at a given pressure to the k_{sat} of the same sample i , $\mu_{\{n,i,t,s\}}$ is the latent relative conductivity that is considered as the true value for the combination $\{n, i, t, s\}$, and σ_y^2 is measurement error variance.

Stage 2 Process model. The latent conductivity for each measurement is centered at the $relK$ predicted by reparameterized Weibull function.

$$\begin{aligned} \mu_{\{n,j,t,s\}} &\sim N(relK_{\{n,i,t,s\}}, \sigma_\mu^2) \\ relK_{\{n,i,t,s\}} &= f(P_{50\{i,t,s\}}, S_{50\{i,t,s\}}, k_{sat\{i,t,s\}} | P_{\{n,i,t,s\}}) \end{aligned} \quad (5)$$

where $f(\cdot)$ is the reparameterized Weibull (Eq 3), and σ_μ^2 is process error variance. Following the model configuration by Ogle *et al.*, process error adopts a nonconstant form depending on $relK$ so that the error is maximized when $relK = 0.5$ whereas minimized when $relk = 0$ or 1 :

$$\sigma_{\mu\{n,i,t,s\}}^2 = \sigma_P^2 \cdot \left(\frac{relK_{\{n,i,t,s\}}(1 - relk_{\{n,i,t,s\}})}{0.25} \right) \quad (6)$$

where $relK_{\{n,j,t,s\}}$ is the relative conductivity defined in (Eq 5). This nonconstant form assumes that there is greater stochasticity and uncertainty when xylem is half-functional, whereas all uncertainty at the two extremes is attributed to measurement error σ_y^2 (Ogle *et al.*, 2009).

Stage 3 Parameter model. Three hydraulic parameters P_{50} , S_{50} , and k_{sat} in Eq 5 were modelled to follow a multivariate normal distribution:

$$\begin{bmatrix} P_{50\{i,t,s\}} \\ S_{50\{i,t,s\}} \\ k_{sat\{i,t,s\}} \end{bmatrix} \sim MVN \left(\begin{bmatrix} \bar{P}_{50\{t,s\}} \\ \bar{S}_{50\{t,s\}} \\ \bar{k}_{sat\{t,s\}} \end{bmatrix}, \Sigma_{\{t\}} \right) \quad (7)$$

where $\bar{P}_{50\{t,s\}}$, $\bar{S}_{50\{t,s\}}$, $\bar{k}_{sat\{t,s\}}$ are the means for organ t of species s , $\Sigma_{\{t\}}$ is covariance matrix for organ t and is decomposed to:

$$\Sigma_{\{t\}} = \text{diag} \begin{bmatrix} v_{P_{50\{t\}}}^2 \\ v_{S_{50\{t\}}}^2 \\ v_{k_{sat\{t\}}}^2 \end{bmatrix} \times \Omega_{\{t\}} \times \text{diag} \begin{bmatrix} v_{P_{50\{t\}}}^2 \\ v_{S_{50\{t\}}}^2 \\ v_{k_{sat\{t\}}}^2 \end{bmatrix} \quad (8)$$

where $v_{\cdot\{t\}}^2$ is variance for a hydraulic parameter in organ t , and $\Omega_{\{t\}}$ is correlation matrix for organ t .

Each mean in Eq 7 is determined by organ effect (α), organ effect (β), and the interaction between organ effect and species (γ).

$$\begin{aligned}
\bar{P}_{50\{t,s\}} &= \mu_{P_{50}} + \alpha_{P_{50}\{s\}} + \beta_{P_{50}\{t\}} + \gamma_{P_{50}\{t,s\}} \\
\bar{S}_{50\{t,s\}} &= \mu_{S_{50}} + \alpha_{S_{50}\{s\}} + \beta_{S_{50}\{t\}} + \gamma_{S_{50}\{t,s\}} \\
\bar{k}_{sat\{t,s\}} &= \mu_{k_{sat}} + \alpha_{k_{sat}\{s\}} + \beta_{k_{sat}\{t\}} + \gamma_{k_{sat}\{t,s\}}
\end{aligned} \tag{9}$$

With data on $A_s:A_L$, LSC for species s is centered around species mean:

$$LSC_{\{s\}} \sim N(\bar{LSC}_{\{s\}}, \nu_{LSC_{\{s\}}}^2) \tag{10}$$

For species effects α, β, γ , sum-to-zero constraints were imposed as in a typical ANOVA.

$$\sum_{s=1}^S \alpha_{\{s\}} = \sum_{t=1}^T \beta_{\{t\}} = \sum_{s=1}^S \gamma_{\{t,s\}} = \sum_{t=1}^T \gamma_{\{t,s\}} = 0 \tag{11}$$

Lemoine (2019) advocates a gradual shift from noninformative to weakly informative priors when implementing Bayesian models in ecology to regularize results and reduce the risk of false positive (type I error) and overestimated effect size (type M error). Here we used weakly informative normal distribution that are centered at zero for grand means and three effects with variances depending on the scale and generally known ranges of P_{50} , S_{50} , and k_{50} .

$$\mu, \alpha_{\{s\}}, \beta_{\{t\}}, \gamma_{\{t,s\}}, \bar{LSC}_{\{s\}} \sim N(0, A^2) \tag{12}$$

where $A = 5$ for P_{50} , k_{sat} , and $\bar{LSC}_{\{s\}}$, while $A = 20$ for S_{50} .

Following one possible choice suggested by Lemoine (2019), all standard deviations (σ_P, σ_y, ν) have half-Cauchy($0, 2.5$) as a weakly informative prior to modestly regularize the results from low-powered data without compromising high-powered data. The two correlation matrices have Lewandowski-Kurowicka-Joe (LKJ) distribution with $\eta = 2$ as the prior. If $\eta = 1$, the density is uniform over all elements in correlation matrix; if $\eta > 1$, the diagonal has higher density(Stan Development Team, 2021).

The BH model in the present study was implemented and sampled with 8 parallel chains and 5000 iterations per chain in Stan version 2.28 via the interfaces “CmdStanR” and “RStan”. To compare with observations, VCs were plotted using posterior means of parameters, and PLC was calculated by assuming that maximum k_s to equal to k_{sat} of each sample. In the strict sense, these two values are not the same in the Bayesian model, because as a free parameter, k_{sat} is random with an associated probability distribution instead of a fixed value.

Daily Canopy Conductance Index

For each species, six trees were installed with a Grainer-type thermal dissipation probe (TDP) on the main on the main stem below breast height. Although TDPs were installed at several depths, we only used sap flux density in the outer xylem to calculate the index, because it is higher and more sensitive to environmental variation, especially drought (Phillips *et al.*, 1996). Data were collected from the probes for every 15 minutes. The software Baseline (Oishi *et al.*, 2016) was used to process the data on temperature difference between two thermocouples. To determine nightly baseline points as no flow, automatic low-VPD baselining function was used, followed by manual inspection and re-choosing if necessary. Given the baseline points, spikes that would represent measurement error were removed and the gaps were filled by linear interpolation. Then a unitless K value was computed as follows:

$$K = \frac{dT_{max} - dT}{dT}$$

where dT_{max} is the nightly baseline value for each day when there is no flow, and dT is the temperature difference at a given time. Gaps in the output K values from Baseline were filled using simple regressions on other sensors producing similar dynamics at that same time. The K values were then converted to sap flux density (F_d) in $\text{g m}^{-2} \text{ s}^{-1}$ following Granier (1985):

$$F_d = 119 \times K^{1.231}$$

Daily mean sap flux density (\bar{F}_d) was calculated from dawn to dawn, which was defined as the first time within a day when photosynthetically active radiation exceeded $10 \mu\text{mol m}^{-2} \text{ s}^{-1}$. PAR was measured at the same 15 min interval as TDPs. The resulting \bar{F}_d was scaled to $\text{g cm}^{-2} \text{ day}^{-1}$. Canopy transpiration scaled from sap flux density computed with the Granier equation was shown to match well with hydrologic balance in a *P. taeda* stand (Schäfer *et al.*, 2002). Thus, the original parameters were used to calculate index on canopy conductance in the present study.

Relative humidity (RH) was also measured at the same interval and converted to vapor pressure deficit (VPD):

$$VPD = 0.61078 \times e^{\frac{17.27 \times T}{247.3 + T}} \times \left(1 - \frac{RH}{100}\right)$$

where T is temperature in $^{\circ}\text{C}$. To account for difference in daytime length, we normalized VPD in kPa as follows:

$$VPD_z = VPD \times \frac{D}{24 \text{ hours}}$$

where D is the length of daytime ($\text{PAR} > 10 \mu\text{mol m}^{-2} \text{ s}^{-1}$) in hours. Daily canopy conductance index (G_cJ) in $\text{g cm}^{-2} \text{ day}^{-1} \text{ kPa}^{-1}$ was calculated as the ratio of \bar{F}_d to VPD_z , after VPD_z values below 0.1 kPa had been removed to avoid spuriously high G_cJ on a rather humid day. The data on sap flux density and VPD_z used in the present study ranged from April 1 to November 12, 2019. To demonstrate drought conditions at the

site during the same period, we obtained from gridMET through ClimateEngine short-term drought indicator blend (STDIB), which is computed by National Oceanic and Atmospheric Administration. STDIB is a weighted average of Palmer drought severity index, Palmer z-index, 1-month and 3-month standardized precipitation index and is intended to approximate impacts over several days to a few months (NOAA Climate Prediction Center).

Estimating In Situ Root PLC

Soil Water Content

To estimate in situ root PLC (PLC_{root}) during the same period as $G_c I$, we first estimated soil matric potential, which was considered to be equivalent to soil water potential (Ψ_s) in the present study. For *P. echinata*, *P. taeda* PT1 and PT2, a water content reflectometer (30 cm) was inserted into the soil surrounding one of the sap flux trees with TDPs to measure volumetric water content (θ). Another reflectometer was installed for *P. palustris* that was outside the plot grid. Soil water content was measured at the same 15 min interval as all the other sensors described above, and daily average was used for following analyses.

Soil Water Potential

Five soil samples were taken in each species plot within the plot grid (i.e. a total of 30) and another five samples in the outside plot where *P. palustris* were growing. Soil texture in terms of sand, silt, clay fractions (SSC) was determined by hydrometer method. Because the plot grid had a constant spacing, we used ordinary kriging to interpolate soil texture at all sap flux trees except for *P. palustris*. Mean soil texture of the five samples was used for the outside *P. palustris* plot. Given the texture, we used the version of ROSETTA modified by Zhang and Schaap (2017) to estimate parameters for soil water characteristics curve (SWCC) in the form of van Genuchten equation, which relates θ and matric potential. ROSETTA also provides estimates on saturated soil water conductivity, from which unsaturated water conductivity (k_{soil}) can be derived using van Genuchten equation. From here, we estimated Ψ_s through two approaches.

Method 1. Site average Ψ_s and species PLC_{root}

Measurements on θ at each of the four reflectometers were input to the SWCC at the reflectometer, resulting in four series of estimates on Ψ_s . The four Ψ_s on each day were averaged to generate one value of Ψ_s . This one series of values was used to derive PLC_{root} using the posterior mean of VC parameters for each species. Since VC appeared to underestimate PLC in roots at high potentials from -1 to 0 MPa, we

fitted linear regression for each species between -2 and 0 MPa. Both species effect and the interaction between species and water potential in a multiple linear regression turned out significant ($P<0.001$), so simple linear regression was fitted for species separately. Then *in situ* root PLC was estimated as follows:

$$PLC(\Psi_s) = \begin{cases} \max[f(\Psi_s), g(\Psi_s)], & -3 \leq P \leq 0 \\ f(\Psi_s), & P < -3 \end{cases}$$

where Ψ_s is soil water potential, $f(\cdot)$ is Weibull function in Eq (3) with posterior means as the parameters, and $g(\cdot)$ is linear regression fitted with PLC between -2 and 0 MPa.

Method 2. Tree specific Ψ_s and species mean PLC_{root}

Alternatively, for each sap flux tree, data on θ from the reflectometer that had the most similar soil texture to the texture surrounding the tree were input to the SWCC that was specific to the texture around the tree. Similarity in texture was determined by the Euclidean distance in a feature space of SSC. PLC_{root} was estimated using the same piecewise function described above, and species mean PLC_{root} was computed. For *P. palustris*, sap flux trees were not planted on a spatially referenced grid, so one series of PLC_{root} based on its plot average Ψ_s was computed.

Response of Canopy Conductance Index to Root Cavitation

First, we fitted a linear model of G_cJ explained VPD_z, species effect, and the interaction between the two on the linear-log scale in the same form as the function for modelling stomatal conductance versus VPD in Oren *et al.* (1999). The interaction term turned out to be significant ($P=0.001$) and was retained, resulting in a linear model with varying slopes and intercepts across species. The residuals in G_cJ unexplained by $\ln(VPD_z)$ were regressed on $\ln(PLC_{root})$, species effect, and the interaction term. The interaction term was significant in both two methods of computing Ψ_s ($P<0.001$ for both), and Tukey test was performed on coefficients of $\ln(PLC_{root})$. Given significant interaction, simple linear regression of the residual on $\ln(PLC_{root})$ was fitted for each species to calculate coefficient of determination for each species separately. Plausible outliers to the regression were identified by filtering for dates on which we observed $PLC_{root} < 2.5$ using site average Ψ_s (Method 1) and residual < -5 for any species except for *P. echinata*. This species was excluded, because it had rather low PLC_{root} throughout the period, and more negative residuals during drought that were close to regression line would otherwise be misidentified as outliers. We also fitted a linear model of G_cJ explained by $\ln(VPD_z)$, $\ln(PLC_{root})$, species effect, and all second-order interaction terms to determine the relative importance for $\ln(VPD_z)$ and $\ln(PLC_{root})$ using the package “relaimpo” (Grömping, 2015). The Lindemann-Merenda-Gold (LMG) metric used reflects sequential R^2 partitioning among variables averaged over all possible orderings of regressors.

Results

Vulnerability Curves

Frequentist and Bayesian approaches yielded similar point estimates for P_{50} and k_{sat} but not for S_{50} (Fig S1-3). The two approaches adopt different ways to quantify uncertainty, so it is inappropriate to directly compare in the present study estimates of uncertainty by the two approaches. The Bayesian approach took into account variation and effects on parameters at different levels and therefore was used to present results below.

In general, branches of all species had a posterior mean P_{50} of -5.71 MPa with 95% credible interval of [-5.92, -5.52] and were far more negative than roots (-2.79 MPa, [-3.03, -2.55]). S_{50} was similar in branches (-46.0 % MPa⁻¹ [-50.9, -41.5]) and roots (-44.8 % MPa⁻¹, [-53.3, -37.0]). k_{sat} was much lower in branches (1.25 kg m⁻¹ s⁻¹ MPa⁻¹, [1.10, 1.39]) than in roots (7.97 kg m⁻¹ s⁻¹ MPa⁻¹, [6.94, 8.99]). Correlation coefficient between any pair of above three hydraulic parameters was unlikely to distinctly deviate from zero, but roots had less uncertainty and were more likely than branches to have a fairly weak negative correlation between P_{50} and k_{sat} (Fig 1H, I).

Across species, P_{50} was quite similar in branches, except that *P. echinata* was likely to have the most negative value, whereas *P. taeda* PT2 the least negative P_{50} (Fig 1A). Despite the uncertainty, there appeared to be a trend toward more negative P_{50} in roots with decreasing needle length, except for *P. taeda* PT2 that had less negative P_{50} than expected by the trend (Fig 1B). The two short-needle species, *P. virginiana* and *P. echinata*, had almost the same root P_{50} . S_{50} did not show clear pattern and appeared similar across species, although *P. virginiana* tended to have the least negative S_{50} in branches (Fig 1B, E). *P. taeda* PT2 had the highest k_{sat} in branches followed by *P. taeda* PT1, while *P. virginiana* appeared to be the lowest followed by *P. echinata* (Fig 1C). *P. virginiana* had the highest point estimate on LSC but with large uncertainty, and it seemed that LSC gradually declined with increasing needle length from *P. taeda* PT2 to *P. palustris* (Fig 1G). The two short-needle species did not appear to have similar LSC, with *P. echinata* having a LSC close to *P. elliottii* and *P. palustris*. Finally, root k_{sat} was fairly similar among the species (Fig 1F).

VCs constructed with posterior means of P_{50} , S_{50} , and k_{sat} represented well the PLC that was calculated by assuming maximum k_s as k_{sat} at most water potentials but appeared to underestimate PLC in roots for all species groups at high water potentials from -1 to 0 MPa (Fig 2). By contrast, PLC calculated as above was well fitted by linear regression at this range of high water potentials (Fig 2, Fig S4).

Safety margin, on average, was higher in branches than in roots and did not notably vary in branches across species (Fig 3). However, it had larger variation across species in roots, and *P. echinata* and *P. virginiana* appeared to have the highest safety margin, whereas *P. taeda* PT2 and *P. palustris* the lowest.

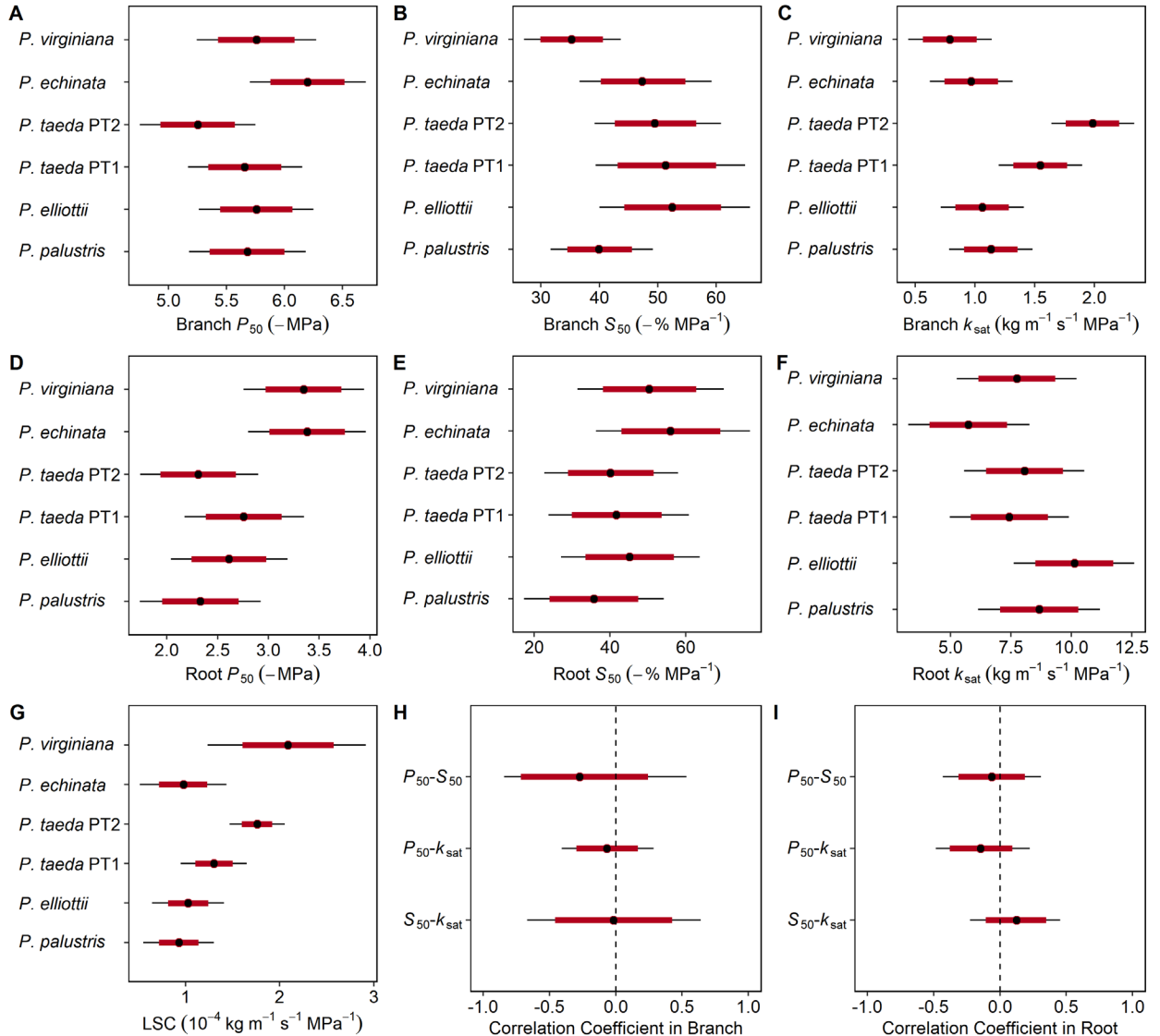


Fig 1. Hydraulic parameters associated with vulnerability curves (VCs) for branches (A-C) and roots (D-F) of *P. virginiana*, *P. echinata*, *P. taeda* PT2, *P. taeda* PT1, *P. elliotii*, and *P. palustris*. (A, D) P_{50} , water potential at which 50% of xylem specific conductivity is lost. (B, E) S_{50} , the slope of VC at P_{50} . (C, F) k_{sat} , xylem specific conductivity. (G) Leaf specific conductivity. (H, I) Correlation coefficients derived from the covariance matrix for P_{50} , S_{50} , k_{sat} in branches and roots respectively. Species are ordered by increasing needle-length from top to bottom. Black points present posterior means, thickened segments represent 80% credible intervals, and line segments represent 95% credible intervals.

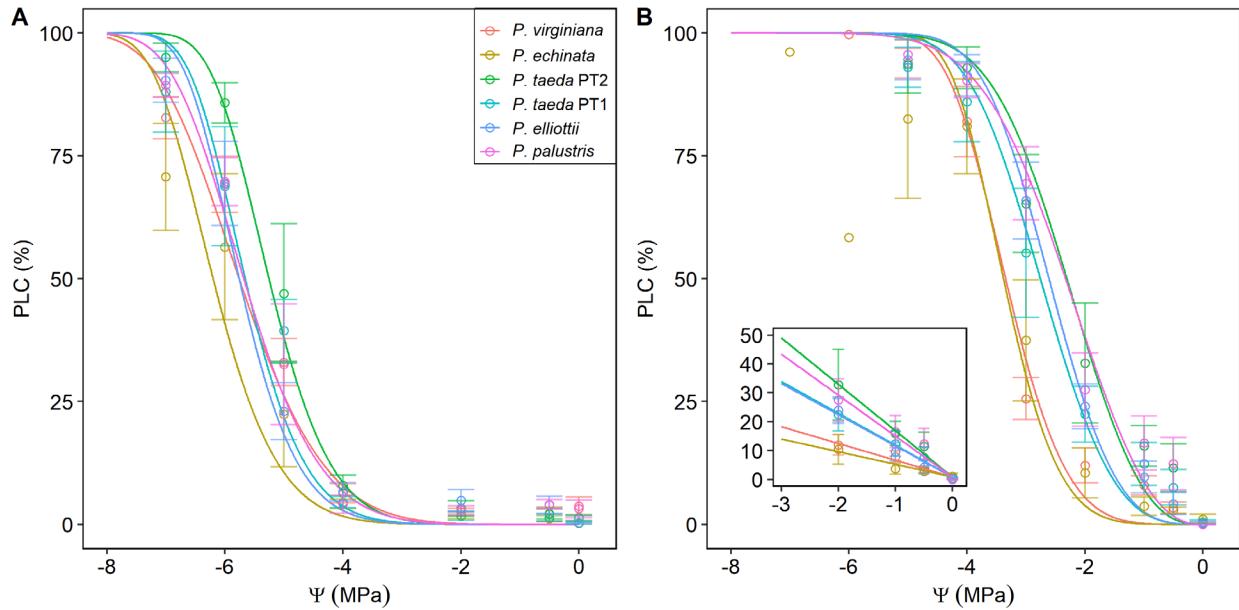


Fig 2. Vulnerability curves (VCs) plotted with posterior means of P_{50} (i.e. water potential at which 50% of xylem specific conductivity is lost) and S_{50} (i.e. the slope of VC at P_{50}) for branches (A) and roots (B) of *P. virginiana*, *P. echinata*, *P. taeda* PT2, *P. taeda* PT1, *P. elliotii*, and *P. palustris*. PLC stands for percent loss of conductivity, and Ψ for water potential. Simple linear regression for roots under high water potentials (-2 to 0 MPa) is shown in the inset. PLC in the figure was calculated by assuming the maximum observed xylem specific conductivity for a sample as its saturated xylem specific conductivity. Points represent sample means, and error bars represent standard errors. The PLCs of root samples that reached water potentials lower than other samples are shown without error bar

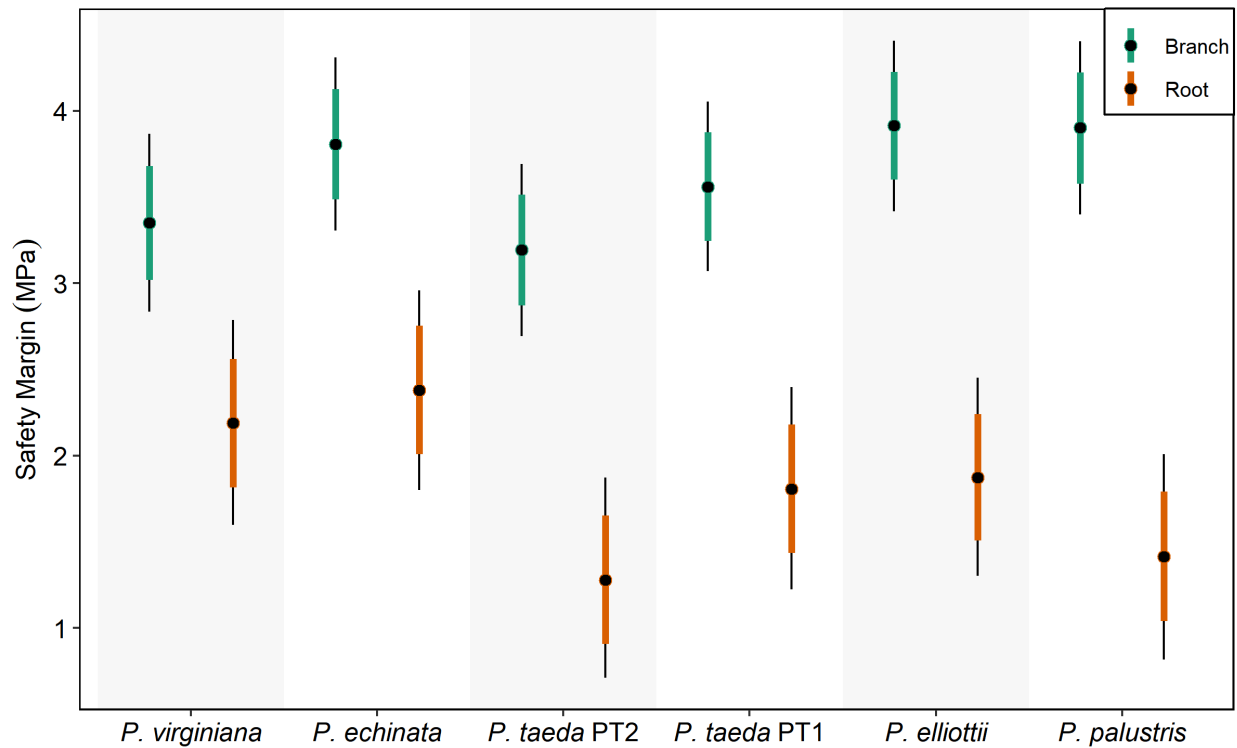


Fig 3. Safety margin in branches and roots of *P. virginiana*, *P. echinata*, *P. taeda* PT2, *P. taeda* PT1, *P. elliottii*, and *P. palustris*. Distribution of safety margin for each species was calculated by subtracting posterior draws of P_{50} (i.e. water potential at which 50% of xylem specific conductivity is lost) by the observed minimum leaf water potentials of the species at predawn for roots and at midday for branches. Leaf water potentials were assumed to be a constant. Species are ordered by increasing needle-length from left to right. Black points present posterior means, thickened segments represent 80% credible intervals, and line segments represent 95% credible intervals.

Environmental Water Conditions and Daily Canopy Conductance Index

Throughout the whole growing season (April to November 2019), the study site experienced two short-term droughts, a minor one around June and a major one around October (Fig 4A). The drought in October lasted longer and was more severe in that the lowest value of the short-term drought indicator blend (STDIB) on October 12 ranked 7.88% since Jan 5, 1980. The dynamics of short-term drought was not well reflected by VPDz (Fig 4B) but was reflected in θ , Ψ_s and k_{soil} (Fig 5A-C). G_cI was also reduced during the two droughts in all species (Fig 4C). Interpolated clay, which has most influence on SWCC, ranged from nearly zero to 23.4%, and the soil around four reflectometers for θ , including the one installed in the separate *P. palustris* plot, ranged from nearly zero to 18.5% in clay fraction (Fig S5). Depending on the method of computing Ψ_s , PLC_{root} had different ranges (Fig 5D, E). Using site average Ψ_s (Method 1 in *Estimating In Situ Root PLC*) produced PLC_{root} below 8% for all species, whereas using tree specific Ψ_s (Method 2) yielded close to 20% in *P. palustris*.

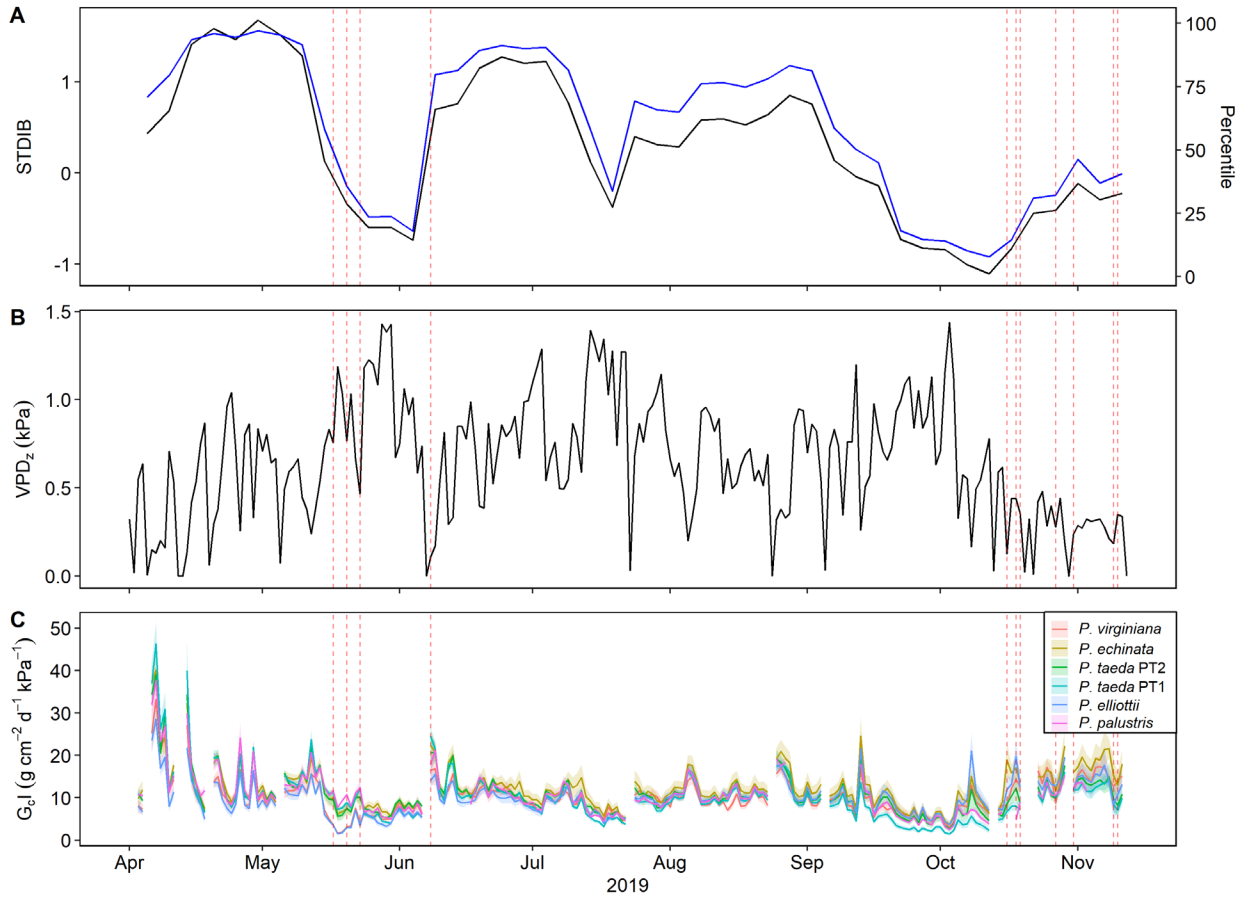


Fig 4. Environmental conditions and Canopy conductance index (G_{cI}) throughout the growing season (April to November) in 2019. (A) Short-term drought indicator blend, which is a weighted average of Palmer drought severity index, Palmer z-index, 1-month and 3-month standardized precipitation index to reflect impacts over several days to a few months. The blend was designed and computed by National Oceanic and Atmospheric Administration and retrieved for the study site based on coordinates. The black line represents the actual value of the blend, while the blue line represents percentile rank since Jan 5, 1980. (B) Vapor pressure deficit normalized by daytime length. (C) G_{cI} of *P. virginiana*, *P. echinata*, *P. taeda* PT2, *P. taeda* PT1, *P. elliottii*, and *P. palustris*. Dashed red lines indicate occasions of plausible outliers for the residual regression of G_{cI} to the estimated *in situ* percent loss of conductivity in roots (PLC_{root}). Ribbons in (C) represent standard errors calculated with sap flux trees. See the Methods section *Daily Canopy Conductance Index* for definition of G_{cI} .

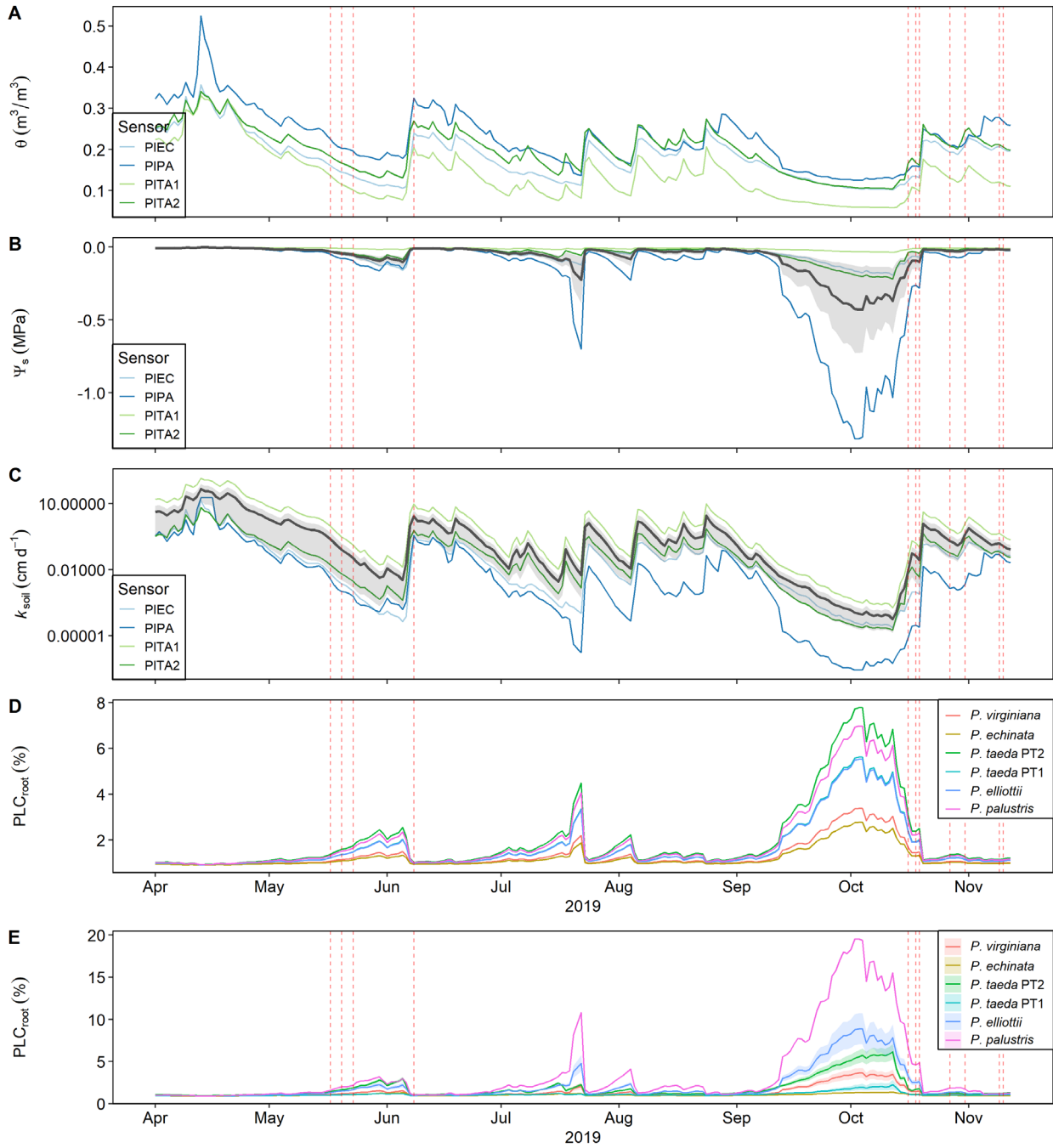


Fig 5. Soil water conditions and the estimated *in situ* percent loss of conductivity in roots (PLC_{root}). (A) Soil water content (θ). (B) Soil water potential (Ψ_s) estimated from θ at four reflectometers depending on the interpolated soil texture at each reflectometer. Thick gray lines represent site average Ψ_s , which is the average of the Ψ_s at four reflectometers. (C) Unsaturated soil water conductivity estimated in the same way as (B). (D) PLC_{root} estimated using site average Ψ_s (Method 1). (E) PLC_{root} estimated using tree-specific Ψ_s (Method 2). Ribbons represent standard errors. No ribbon is shown for *P. palustris*, because its PLC_{root} was computed with one plot average Ψ_s . Dashed red lines indicate occasions of plausible outliers for the residual regression of $G_{\text{c}}I$ to PLC_{root}. See the Methods section *Soil Water Potential* for detailed explanation on the two methods used in (D) and (E).

Response of Canopy Conductance Index to Root Cavitation

When simultaneously considering VPD_z, PLC_{root} derived from site average Ψ_s , species effect, and interactions in a linear-log relationship, VPD_z accounted for 66.5% of the total variance explained by the full model ($R^2 = 0.756$, $P < 0.001$), while PLC_{root} accounted for 23.9%. By contrast, species effect and all second-order interactions accounted for less than 4%. Similarly, using tree specific Ψ_s , VPD_z accounted for 70.3% of total explained variance ($R^2 = 0.742$, $P < 0.001$), while PLC_{root} for 15.4%, and all the others for less than 7%. In the residual regression, PLC_{root} derived from site average Ψ_s accounted for 83.6% of the total explained variance ($R^2 = 0.277$, $P < 0.001$), and the variation in its slope among species groups for 12.6%. PLC_{root} derived from tree specific Ψ_s accounted for 51.7% of the total explained variance ($R^2 = 0.269$, $P < 0.001$), and the variation in the slope for 41.0%.

When considering each species separately using site average Ψ_s , the proportion of variance in $G_c I$ residual that was explained by PLC_{root} varied across species (0.055-0.378), and PLC_{root} explained the least proportion of variance in *P. elliottii* (Fig 6). *P. virginiana* and *P. echinata* appeared to have sensitivities to PLC_{root} (i.e. the slope associated with ln(PLC_{root})) that were similar to each other and also other species except for *P. elliottii*, which was most insensitive. The two variants of *P. taeda* that had different crown shapes did not have similar slopes. If tree specific Ψ_s was used, species manifested greater variation in sensitivity to PLC_{root}, and *P. echinata* and *P. taeda* PT1 had the highest sensitivity, while *P. elliottii* still had the lowest sensitivity, and the other three species intermediate sensitivity (Fig 7, Fig S6).

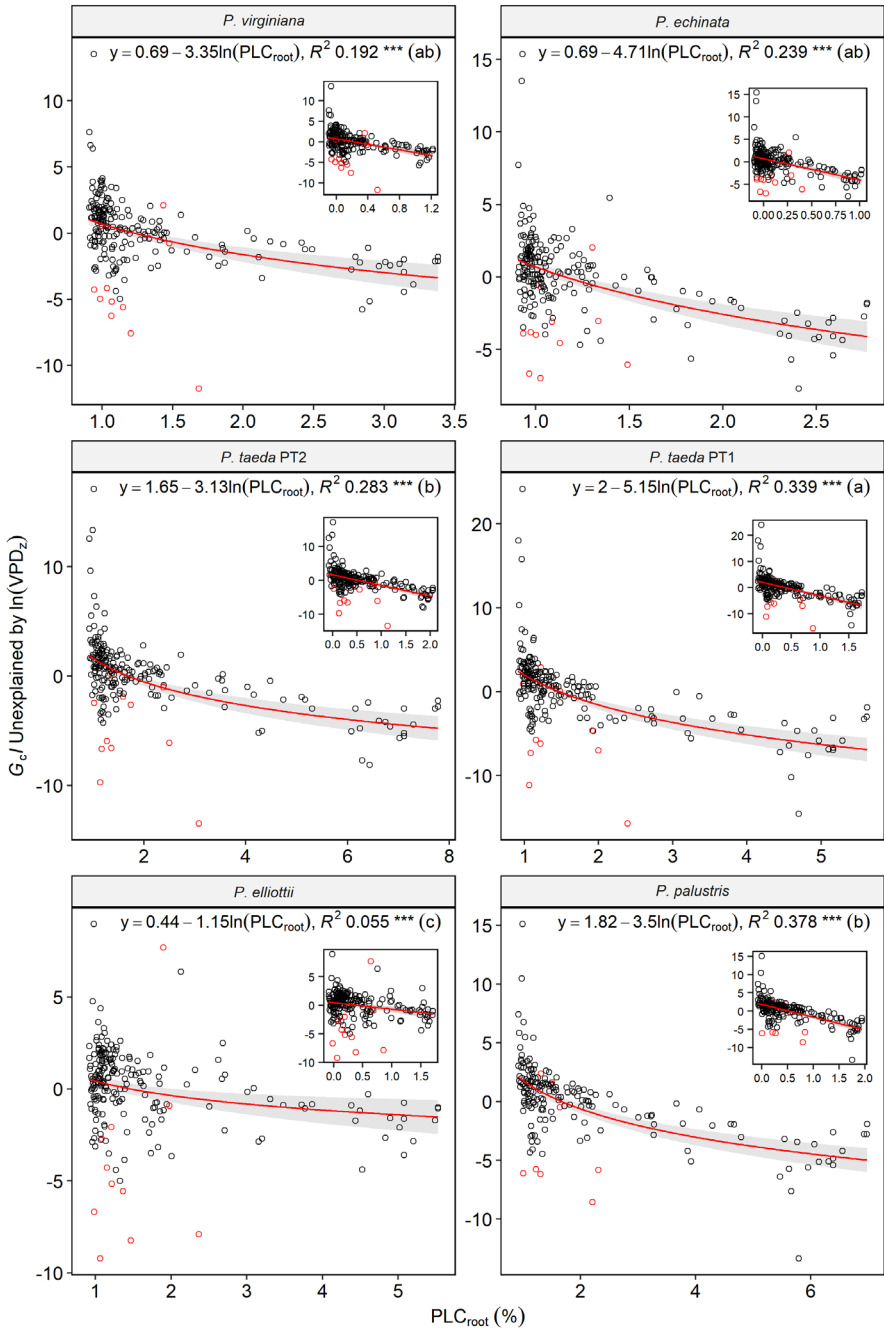


Fig 6. Regression of residual in canopy conductance index (G_cJ) unexplained by normalized vapor pressure deficit (VPD_z) on the estimated *in situ* percent loss of conductivity in roots (PLC_{root}) using a linear-log relationship. PLC_{root} was derived from site average Ψ_s . Insets show regression and data points on the linear-log scale. P value: *** < 0.001 . Red points indicate occasions of plausible outliers for the regression and correspond to the red dashed lines in Fig 4, 5. Significance letters show results of Tukey test on the slope associated with $\ln(PLC_{root})$ using a full model that included species effect and interaction with the slope. Ribbons represent 95% confidence intervals.

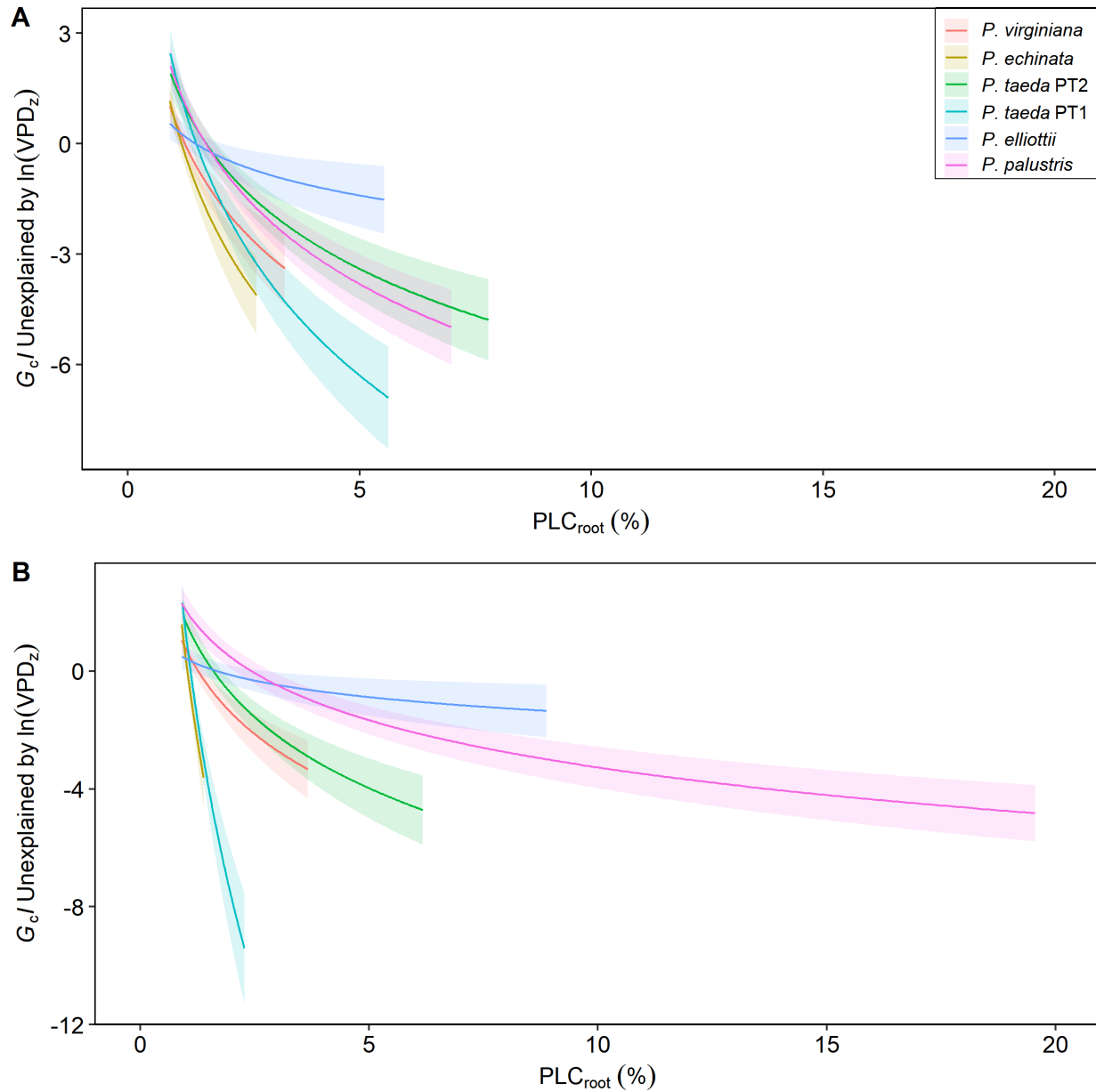


Fig 7. Regression of residual in canopy conductance index ($G_c J$) unexplained by normalized vapor pressure deficit (VPD_z) on the estimated *in situ* percent loss of conductivity in roots (PLC_{root}) using a linear-log relationship. All species are plotted with the same range. (A) PLC_{root} derived from site average soil water potential (Ψ_s). (B) PLC_{root} derived from tree specific Ψ_s . Ribbons represent 95% confidence interval.

Discussion

Hydraulic Parameters

In the present study, we found that branches in all of the studied pine species were more resistant to cavitation and had greater safety margin than roots. The results were in agreement with previous studies. Johnson *et al.* (2016) reported a P_{50} of -3.90 MPa for branches and -1.34 MPa for roots of *P. taeda*, and -3.65 MPa for branch and -1.12 MPa for root of *P. virginiana*. Although their P_{50} values were less negative than ours (Fig 1A, D), their results still suggested that branches of the two species shared similar vulnerability but did not suggest that *P. virginiana* may have more resistant roots than *P. taeda*. Lodge *et al.* (2018) tested vulnerability curves of *P. palustris* under different temperatures and found under ambient P_{50} was -3.55 MPa for branches and -2.08 MPa for roots. *P. echinata* was also found in a previous study to have similar P_{50} in stem (-3.21 MPa) and in roots (-1.47 MPa) (Maherali *et al.*, 2006). Overall, the present study yielded point estimates on P_{50} that were more negative than the existing literature. This is unlikely due to the Bayesian approach employed here, because the VCs plotted with the posterior means of hydraulic parameters follow the general trend of species average PLC at most levels of water potential (Fig 2), except for high water potentials in roots, where deviation is related to the sigmoidal shape of Weibull function and the fact that the function is mathematically forced to pass through the origin (i.e. PLC=0 when $\Psi=0$). Moreover, the frequentist approach still generated point estimates on P_{50} close to the posterior means for all species (Fig S1). Instead, this slight inconsistency might be attributed to detailed protocols to introduce cavitation in samples with the air injection method. Despite the slight difference in experimental procedure across studies, in the present study samples of all species were processed under the same protocol and analyzed in one hierarchical model that accounted for variation and effect at different levels. Therefore, our results should be directly comparable across species. Posterior distributions produced by the Bayesian approach suggests relatively large uncertainty at species level, as indicated by relatively wide credible intervals (Fig 1). The uncertainty may reflect the inherent variation of P_{50} and other hydraulic parameters within species, variation which may be reduced with larger sample size.

Safety margin, defined as the difference between minimal Ψ observed under natural conditions and P_{50} , is commonly used to quantify the extent of hydraulic conservatism in a plant (Choat *et al.*, 2012). Lower safety margin indicates the plant is experiencing higher level of embolism and greater risk of hydraulic failure. We found that all studied species had larger safety margin in branches than in roots, suggesting that roots were consistently at greater risk of hydraulic failure. This pattern is consistent with the results from Johnson *et al.* (2016) on *P. taeda* and *P. virginiana*. Similar to the contrast on P_{50} , their study suggests similar safety margin between the two species, but our results suggest that *P. virginiana* and *P. echinata* were experiencing similar risk in branches but less risk in roots in comparison to other

species (Fig 3). Notably, safety margin in roots of *P. echinata* even had some overlap with that in branches of *P. taeda* PT2.

Unlike P_{50} , k_{sat} was very similar in roots, but appeared to have a decreasing trend with shorter needle length (Fig 1C, F). However, if the specific conductivity is considered on the basis of per unit leaf area, then *P. virginiana* appeared to have greater value but with large variation (Fig 1G). LSC is a measure of the capability of xylem to supply water to leaves that are downstream along water transport pathway. *Pinus sylvestris* has been found to decrease LSC where dry conditions prevail as a result of smaller sapwood area, smaller diameter of conduits, and greater reduction in stem conductivity than in leaf area (Sterck *et al.*, 2008). In the present study, we did not investigate the change in LSC among these species along a gradient of water conditions, but lower LSC in species other than *P. virginiana* may suggest that they were under greater pressure from the same environmental conditions of the common garden. However, it should also be noted that *P. virginiana* had fairly large uncertainty in LSC and did not deviate markedly from other species.

As a classic hypothesis, the efficiency-safety tradeoff has been tested across various species in different biomes (Gleason *et al.*, 2016; Sande *et al.*, 2019; Liu *et al.*, 2021). Most of these studies examined such a relationship across species, but in the present study we tested it in branches and roots separately at the sample level. There was not strong evidence for the tradeoff in both branches and roots among the six species, although roots were more likely to manifest a tradeoff between P_{50} and k_{sat} (Fig 1H, I). This may suggest that variations in safety trait and efficiency trait are not strongly negatively correlated with each other at individual segment of organ or at individual tree level, and thus benefits brought by plasticity in one trait may not necessarily coupled with comprise in another. However, study using samples from a gradient of water conditions is needed to fully investigate the tradeoff at the level of individual trees in branches and roots.

Soil Water Conditions and Response of Canopy Conductance Index to Root Cavitation

In previous studies in the same region that also entailed estimation on soil water potential (Ψ_s) (e.g. Ewers *et al.*, 2000; Hacke *et al.*, 2000), parameters for soil water characteristic curve (SWCC) were usually taken from another study that had similar qualitative soil texture (e.g. sandy loam). In the present study, we used a model (ROSETTA) that estimates these parameters based on the numeric fraction of sand, silt, and clay. Combined with interpolated soil texture for the whole site, this method allowed us either to follow previous studies by using one Ψ_s for the entire study site for each day (Method 1 in Methods section), or to estimate Ψ_s at each tree that was installed with thermal dissipation probes for sap flux density (Method 2). The latter may better reflect microsite variability in soil texture (Fig S5) but at the same time may be confounded by the error introduced by measurement and interpolation of soil texture.

Moreover, reflectometers for soil water content were installed at four locations, not near each sap flux tree, and a reflectometer was selected to represent the conditions near each sap flux tree depending on similarity in soil texture. The texture near the four reflectometers did not cover the entire range of texture surrounding sap flux trees. Furthermore, similarity was estimated by Euclidean distance in the feature space of soil texture, but each of the three mineral components has unequal impact on the behavior of SWCC, with clay having disproportionately large impact. Thus, another more appropriate distance that can account for the unequal impact may need to be devised. With site average Ψ_s , it was assumed that all the trees in the study site were experiencing the same water condition, and any difference among species in the response of canopy conductance to root cavitation can be attributed to difference intrinsic to species. By contrast, with tree specific Ψ_s , it was assumed that the difference in soil water conditions among different microsites was also involved and should be taken into account.

The most widely accepted method to calculate canopy conductance is using inverse Penman-Monteith equation and was approximated by a simplified method that uses sap-flux-scaled evapotranspiration (Ewers & Oren, 2000). In the present study, we used an even more simplified index that did not involve measurement on the ratio of sapwood area to leaf area but instead directly used daily integrated sap flux density as a measure of transpiration. This method allowed us to continuously monitor relative change in canopy conductance, represented by G_cI , at a temporal scale commensurate with changes in soil moisture.

Regardless of the way to estimate Ψ_s , we found that variance in canopy conductance index (G_cI) that was not explained by vapor pressure deficit normalized by daytime length (VPD_d) can be explained to a notable extent by water conditions in roots, as represented by estimated *in situ* PLC in root (PLC_{root}; Fig 6, 7, S6). Although G_cI is not the same as the canopy conductance, G_cI was well fitted using a linear-log relationship with VPD (Fig S7), a relationship that was shown to be consistent with stomatal role in protecting the hydraulic function of the xylem (Oren *et al.*, 1999). When fitting the residual regression on PLC_{root}, we still employed the linear-log form, and residuals were well represented in all species (Fig 6).

With site average Ψ_s , all species had similar sensitivity to PLC_{root}, except for the most insensitive *P. elliottii*. However, comparing the regression line at the same level of PLC_{root}, *P. virginiana*, *P. echinata*, and *P. taeda* PT1 had lower G_cI than other species, suggesting the three species might employ a more conservative hydraulic strategy to preserve water by reducing canopy conductance (Fig 7A). Moreover, *P. virginiana* and *P. echinata* had more resistant roots, as suggested by both P_{50} and the range of PLC_{root} than *P. taeda* PT1. In contrast, with tree specific Ψ_s , *P. echinata* and *P. taeda* PT1 were most sensitive to PLC_{root}, whereas *P. elliottii* was still the most insensitive (Fig 7B, 6S). However, given that each tree was assumed to experience different soil water conditions, the range of PLC_{root} was not comparable across species.

The P_{50} discussed in the previous section is related to the ultrastructure of xylem and bordered pits in gymnosperm (Delzon *et al.*, 2010). Therefore, it is supposed to determine the capability to withstand droughts without direct compromise on the physiological function of plants, except for the efficiency-safety efficiency. However, reduction in canopy conductance also limits diffusion of CO₂ and thus photosynthesis rate. Hence, reduced canopy conductance that helps prevent hydraulic failure in the short term could incur carbon starvation in the long term, and the most conservative strategy may not lead to the highest survival. The response of canopy conductance should be interpreted within a time frame comparable to the length of droughts. In the present study, the two droughts lasted less than one month, and thus the negative impact of conservative strategy in regulation canopy conductance may not be obvious.

A few plausible outliers to the residual regression that had both low $G_c I$ and PLC_{root} were identified to occur after rain events during the two short-term droughts (June and October). This may be attributed to the lag in refilling of embolized xylem. Vulnerability curve is time-irrelevant and assumes immediate response in PLC as Ψ increases or decreases, but in reality embolized xylem may take some amount of time beyond a day to restore the conductivity. Canopy conductance during such a refilling period may remain low to facilitate the process. Additionally, water storage in trees may also be replenished during the period.

In conclusion, water conditions in roots can explain a non-negligible proportion of variance in canopy conductance that is not explained by vapor pressure deficit alone. *P. virginiana* and *P. echinata* are likely to tolerate drought better than the other species groups, as a result of roots resistant to cavitation and moderate to conservative strategy to preserve water by reducing canopy conductance. Moreover, the contrast between results derived from two methods of estimating Ψ_s suggests that whether or not microsite variability is accounted for in comparative studies can affect our understanding of species response to environmental conditions and calls attention to the assumption made by researchers about homogeneity in soil texture and resulting soil water conditions.

Acknowledgement

HZ appreciates the opportunity to be enrolled in the Assistantship Program (2019-2020 academic year) of the Nicholas School of the Environment. HZ also appreciates the opportunity to participate in a research project initiated by JCD and RO and to carry out the present project under the invaluable guidance of JCD and RO. In addition, HZ appreciates Chris Maier, Karen Sarsony, and Bob Eaton from US Forest Service Southern Research Station for providing the data on soil texture as well as routine maintenance of the study site.

References

- Choat B, Jansen S, Brodribb TJ, Cochard H, Delzon S, Bhaskar R, Bucci SJ, Feild TS, Gleason SM, Hacke UG, et al. 2012.** Global convergence in the vulnerability of forests to drought. *Nature* **491**(7426): 752-755.
- Clark JS. 2004.** Why environmental scientists are becoming Bayesians. *Ecology Letters* **8**(1): 2-14.
- Damour G, Simonneau T, Cochard H, Urban L. 2010.** An overview of models of stomatal conductance at the leaf level. *Plant, Cell & Environment*: no-no.
- Delzon S, Douthe C, Sala A, Cochard H. 2010.** Mechanism of water-stress induced cavitation in conifers: bordered pit structure and function support the hypothesis of seal capillary-seeding. *Plant, Cell & Environment* **33**(12): 2101-2111.
- Dixon HH. 1914.** *Transpiration and the ascent of sap in plants*: Macmillan and Company, limited.
- Domec J-C, Gartner BL. 2001.** Cavitation and water storage capacity in bole xylem segments of mature and young Douglas-fir trees. *Tree Physiology* **15**(4): 204-214.
- Duursma R, Choat B. 2017.** fitplc - an R package to fit hydraulic vulnerability curves. *Journal of Plant Hydraulics* **4**: 002.
- Ewers BE, Oren R. 2000.** Analyses of assumptions and errors in the calculation of stomatal conductance from sap flux measurements. *Tree Physiology* **20**(9): 579-589.
- Ewers BE, Oren R, Sperry JS. 2000.** Influence of nutrient versus water supply on hydraulic architecture and water balance in *Pinus taeda*. *Plant, Cell & Environment* **23**(10): 1055-1066.
- Gleason SM, Westoby M, Jansen S, Choat B, Hacke UG, Pratt RB, Bhaskar R, Brodribb TJ, Bucci SJ, Cao K-F, et al. 2016.** Weak tradeoff between xylem safety and xylem-specific hydraulic efficiency across the world's woody plant species. *New Phytologist* **209**(1): 123-136.
- Granier A. 1985.** Une nouvelle méthode pour la mesure du flux de sève brute dans le tronc des arbres. *Annales des Sciences Forestières* **42**(2): 193-200.
- Grömping U. 2015.** Variable importance in regression models. *Wiley Interdisciplinary Reviews: Computational Statistics* **7**(2): 137-152.
- Grossiord C, Buckley TN, Cernusak LA, Novick KA, Poulter B, Siegwolf RTW, Sperry JS, McDowell NG. 2020.** Plant responses to rising vapor pressure deficit. *New Phytologist*.
- Hacke UG, Sperry JS, Ewers BE, Ellsworth DS, Schäfer KVR, Oren R. 2000.** Influence of soil porosity on water use in *Pinus taeda*. *Oecologia* **124**(4): 495-505.
- Hacke UG, Sperry JS, Wheeler JK, Castro L. 2006.** Scaling of angiosperm xylem structure with safety and efficiency. *Tree Physiology* **26**(6): 689-701.
- Johnson DM, Wortemann R, McCulloh KA, Jordan-Meille L, Ward E, Warren JM, Palmroth S, Domec J-C. 2016.** A test of the hydraulic vulnerability segmentation hypothesis in angiosperm and conifer tree species. *Tree Physiology* **36**(8): 983-993.
- Lemoine NP. 2019.** Moving beyond noninformative priors: why and how to choose weakly informative priors in Bayesian analyses. *Oikos* **128**(7): 912-928.
- Lens F, Sperry JS, Christman MA, Choat B, Rabaey D, Jansen S. 2011.** Testing hypotheses that link wood anatomy to cavitation resistance and hydraulic conductivity in the genus *Acer*. *New Phytologist* **190**(3): 709-723.
- Lens F, Tixer A, Cochard H, Sperry JS, Jansen S, Herbette S. 2013.** Embolism resistance as a key mechanism to understand adaptive plant strategies. *Current Opinion in Plant Biology* **16**(3): 287-292.
- Liu H, Ye Q, Gleason SM, He P, Yin D. 2021.** Weak tradeoff between xylem hydraulic efficiency and safety: climatic seasonality matters. *New Phytologist* **229**(3): 1440-1452.
- Lodge AG, Dickinson MB, Kavanagh KL. 2018.** Xylem heating increases vulnerability to cavitation in longleaf pine. *Environmental Research Letters* **13**(5): 055007.

- Maherali H, Moura CF, Caldeira MC, Willson CJ, Jackson RB. 2006.** Functional coordination between leaf gas exchange and vulnerability to xylem cavitation in temperate forest trees. *Plant, Cell and Environment* **29**(4): 571-583.
- Maherali H, Pockman WT, Jackson RB. 2004.** Adaptive variation in the vulnerability of woody plants to xylem cavitation. *Ecology* **85**(8): 2184-2199.
- Martínez-Vilalta J, Prat E, Oliveras I, Piñol J. 2002.** Xylem hydraulic properties of roots and stems of nine Mediterranean woody species. *Oecologia* **133**(1): 19-29.
- Mayr S, Sperry JS. 2010.** Freeze-thaw-induced embolism in *Pinus contorta*: centrifuge experiments validate the ‘thaw-expansion hypothesis’ but conflict with ultrasonic emission data. *New Phytologist* **185**(4): 1016-1024.
- McCulloh KA, Domec JC, Johnson DM, Smith DD, Meinzer FC. 2019.** A dynamic yet vulnerable pipeline: Integration and coordination of hydraulic traits across whole plants. *Plant, Cell & Environment* **42**(10): 2789-2807.
- Neufeld HS, Grantz DA, Meinzer FC, Goldstein G, Crisosto GM, Crisosto C. 1992.** Genotypic variability in vulnerability of leaf xylem to cavitation in water-stressed and well-irrigated sugarcane. *Plant Physiology* **100**(2): 1020-1028.
- Ogle K, Barber JJ, Willson C, Thompson B. 2009.** Hierarchical statistical modeling of xylem vulnerability to cavitation. *New Phytologist* **182**(2): 541-554.
- Oishi AC, Hawthorne DA, Oren R. 2016.** Baseline: An open-source, interactive tool for processing sap flux data from thermal dissipation probes. *SoftwareX* **5**: 139-143.
- Oren R, Sperry JS, Katul GG, Pataki DE, Ewers BE, Phillips N, Schäfer KVR. 1999.** Survey and synthesis of intra- and interspecific variation in stomatal sensitivity to vapour pressure deficit. *Plant, Cell & Environment* **22**(12): 1515-1526.
- Pammenter NW, Van Der Willigen C. 1998.** A mathematical and statistical analysis of the curves illustrating vulnerability of xylem to cavitation. *Tree Physiology* **18**(8-9): 589-593.
- Phillips N, Oren R, Zimmermann R. 1996.** Radial patterns of xylem sap flow in non-, diffuse- and ring-porous tree species. *Plant, Cell and Environment* **19**(8): 983-990.
- Sande MT, Poorter L, Schnitzer SA, Engelbrecht BMJ, Markesteijn L. 2019.** The hydraulic efficiency-safety trade-off differs between lianas and trees. *Ecology* **100**(5): e02666.
- Schäfer KVR, Oren R, Lai C-T, Katul GG. 2002.** Hydrologic balance in an intact temperate forest ecosystem under ambient and elevated atmospheric CO₂ concentration. *Global Change Biology* **8**(9): 895-911.
- Stan Development Team 2021.** Stan Modeling Language Users Guide and Reference Manual, Version 2.28.
- Sterck FJ, Zweifel R, Sass-Klaassen U, Chowdhury Q. 2008.** Persisting soil drought reduces leaf specific conductivity in Scots pine (*Pinus sylvestris*) and pubescent oak (*Quercus pubescens*). *Tree Physiology* **28**(4): 529-536.
- Tyree MT, Sperry JS. 1989.** Vulnerability of Xylem to Cavitation and Embolism. *Annual Review of Plant Physiology and Plant Molecular Biology* **40**(1): 19-36.
- Vilagrosa A, Chirino E, Peguero-Pina J-J, Barigah TS, Cochard H, Gil-Pelegrin E 2012.** Xylem cavitation and embolism in plants living in water-limited ecosystems. In: Aroca R ed. *Plant responses to drought stress*. Berlin, Heidelberg: Springer, 63-109.
- Wheeler JK, Sperry JS, Hacke UG, Hoang N. 2005.** Inter-vessel pitting and cavitation in woody Rosaceae and other vesselled plants: a basis for a safety versus efficiency trade-off in xylem transport. *Plant, Cell & Environment* **28**(6): 800-812.
- Woodruff DR, Meinzer FC, McCulloh KA 2016.** Forest canopy hydraulics. In: Hikosaka K, Niinemets Ü, Anten NPR eds. *Canopy photosynthesis: from basics to applications*: Springer, 187-217.

Zhang Y, Schaap MG. 2017. Weighted recalibration of the Rosetta pedotransfer model with improved estimates of hydraulic parameter distributions and summary statistics (Rosetta3). *Journal of Hydrology* **547**: 39-53.

Supplementary Materials

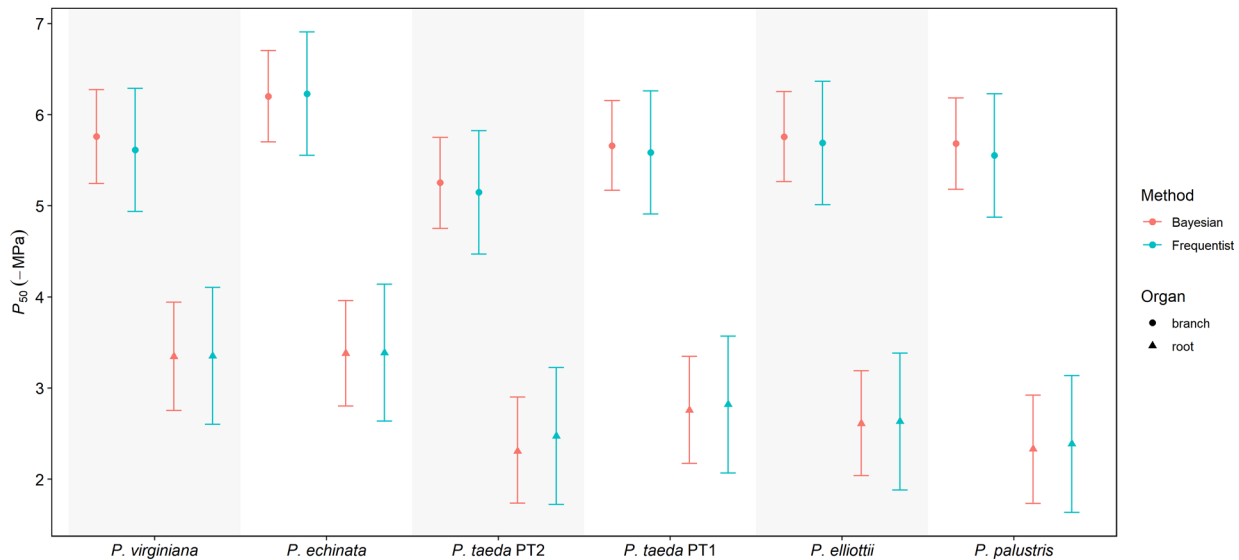


Fig S1. P_{50} estimated by Bayesian and frequentist approaches using the same reparameterized Weibull function. For Bayesian approach, points represent posterior means, and error bars present 95% credible intervals. For frequentist approach, points represent means of P_{50} estimated for each sample and error bars represent 95% confidence intervals adjusted by multivariate t-distribution for multiplicity. Note because the two types of uncertainty intervals have different underlying rationales, they are not directly comparable in the present study.

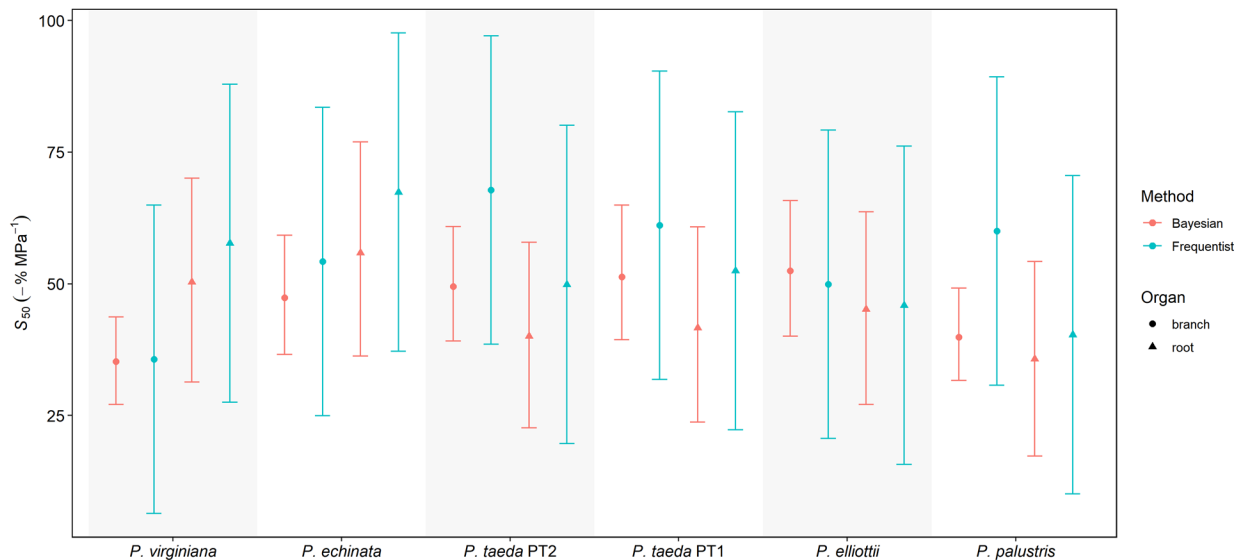


Fig S2. S_{50} estimated by Bayesian and frequentist approaches using the same reparameterized Weibull function. For Bayesian approach, points represent posterior means, and error bars present 95% credible intervals. For frequentist approach, points represent means of P_{50} estimated for each sample and error bars represent 95% confidence intervals adjusted by multivariate t-distribution for multiplicity. Note because the two types of uncertainty intervals have different underlying rationales, they are not directly comparable in the present study.

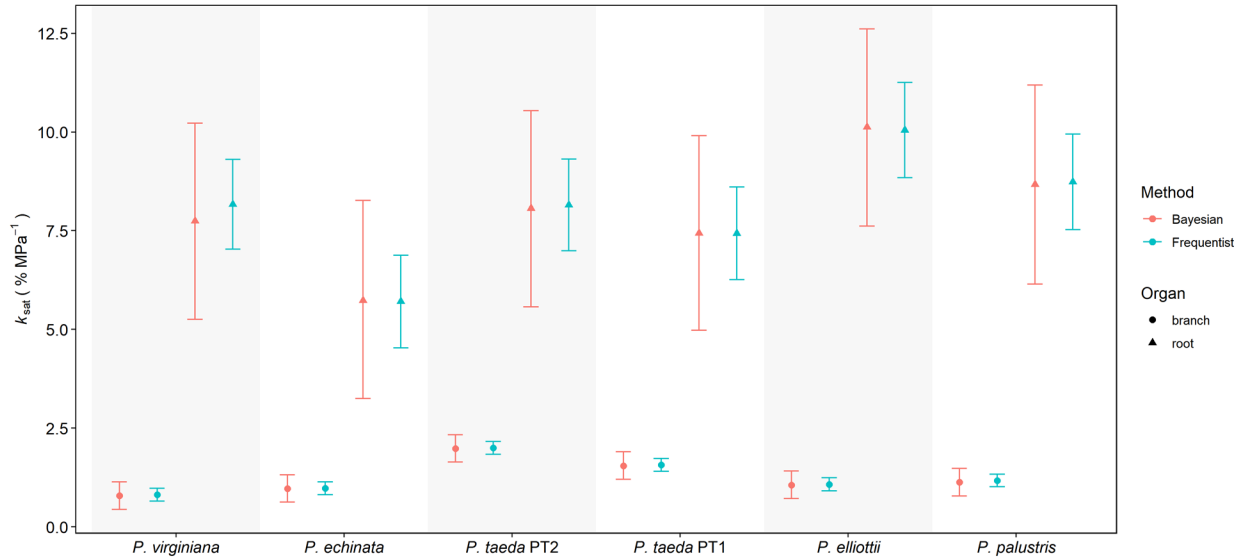


Fig S3. k_{sat} estimated by Bayesian and frequentist approaches using the same reparameterized Weibull function. For Bayesian approach, points represent posterior means, and error bars present 95% credible intervals. For frequentist approach, points represent means of P_{50} estimated for each sample and error bars represent 95% confidence intervals adjusted by multivariate t-distribution for multiplicity. Note because the two types of uncertainty intervals have different underlying rationales, they are not directly comparable in the present study.

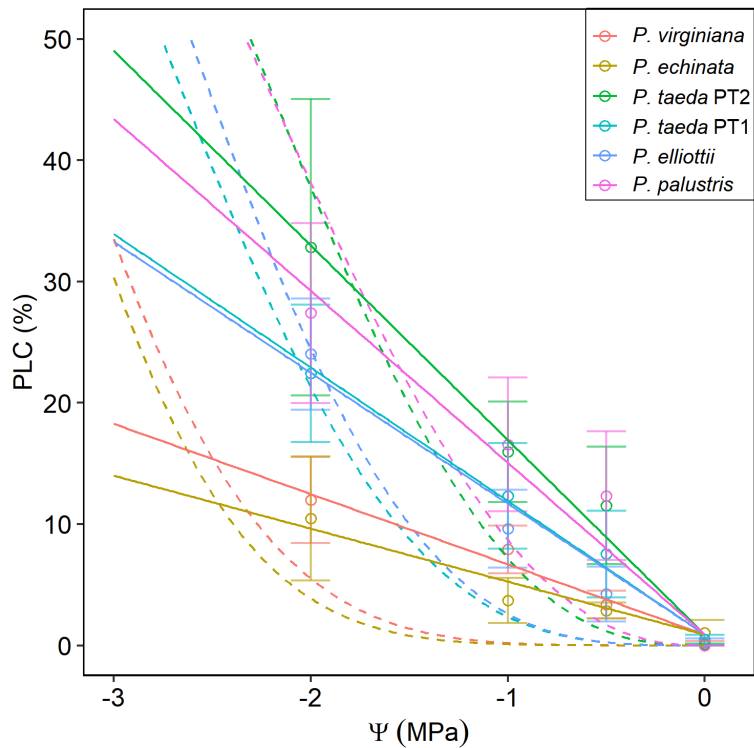


Fig S4. Comparison of vulnerability curves (VCs) fitted with the Bayesian model that used reparameterized Weibull function (dashed lines) and linear regression (solid lines) at high water potentials from -3 to 0 MPa. Percent loss of conductivity (PLC) in the figure was calculated by assuming the maximum observed xylem specific conductivity for a sample as its saturated xylem specific conductivity. Points represent sample means, and error bars represent standard errors.

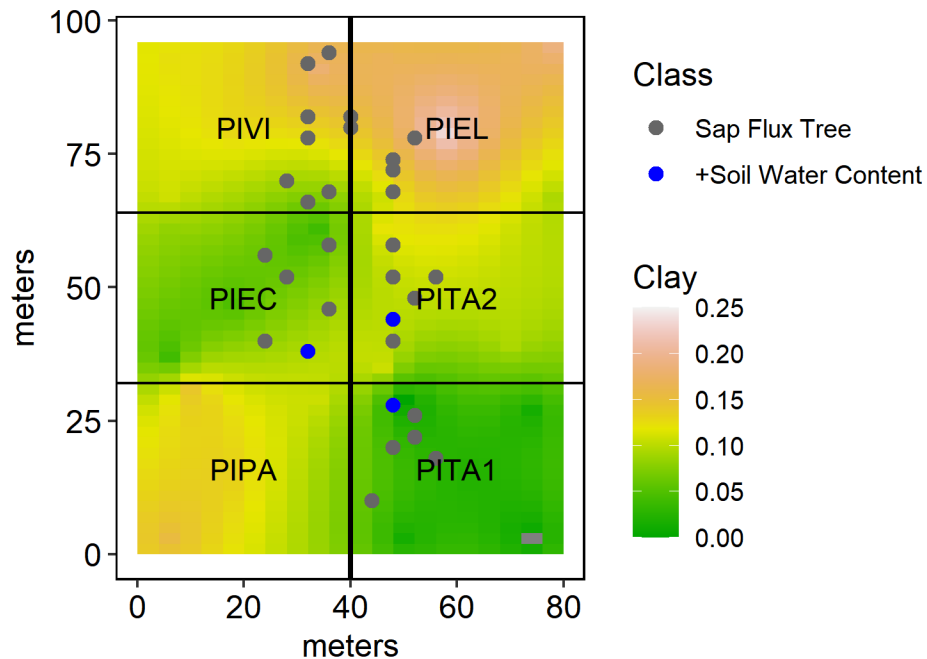


Fig S5. Map of clay fraction interpolated by ordinary kriging for the six species plots. Gray points represent locations of trees installed with thermal dissipation probes (TDPs) for measuring sap flux density. The two other mineral components (sand, silt) were also interpolated similarly but not shown, because clay has the most influence on estimating parameters for the soil water characteristic curve that translates θ to soil water potential and unsaturated soil water conductivity. Blue points represent sap flux tree with a reflectometer installed nearby for soil water content. PIVI – *P. virginiana*; PIEL – *P. elliottii*; PIEC – *P. echinata*; PITA2 – *P. taeda* PT2; PITA1 – *P. taeda* PT1; PIPA – *P. palustris*. Since *P. palustris* seedlings were too young when TDPs were installed, mature trees in a nearby plot were selected for sap flux density measurements. Another reflectometer was installed for the mature *P. palustris* plot. Since the plot did not have a regular spacing, spatial interpolation was not carried out, and plot average texture was used instead.

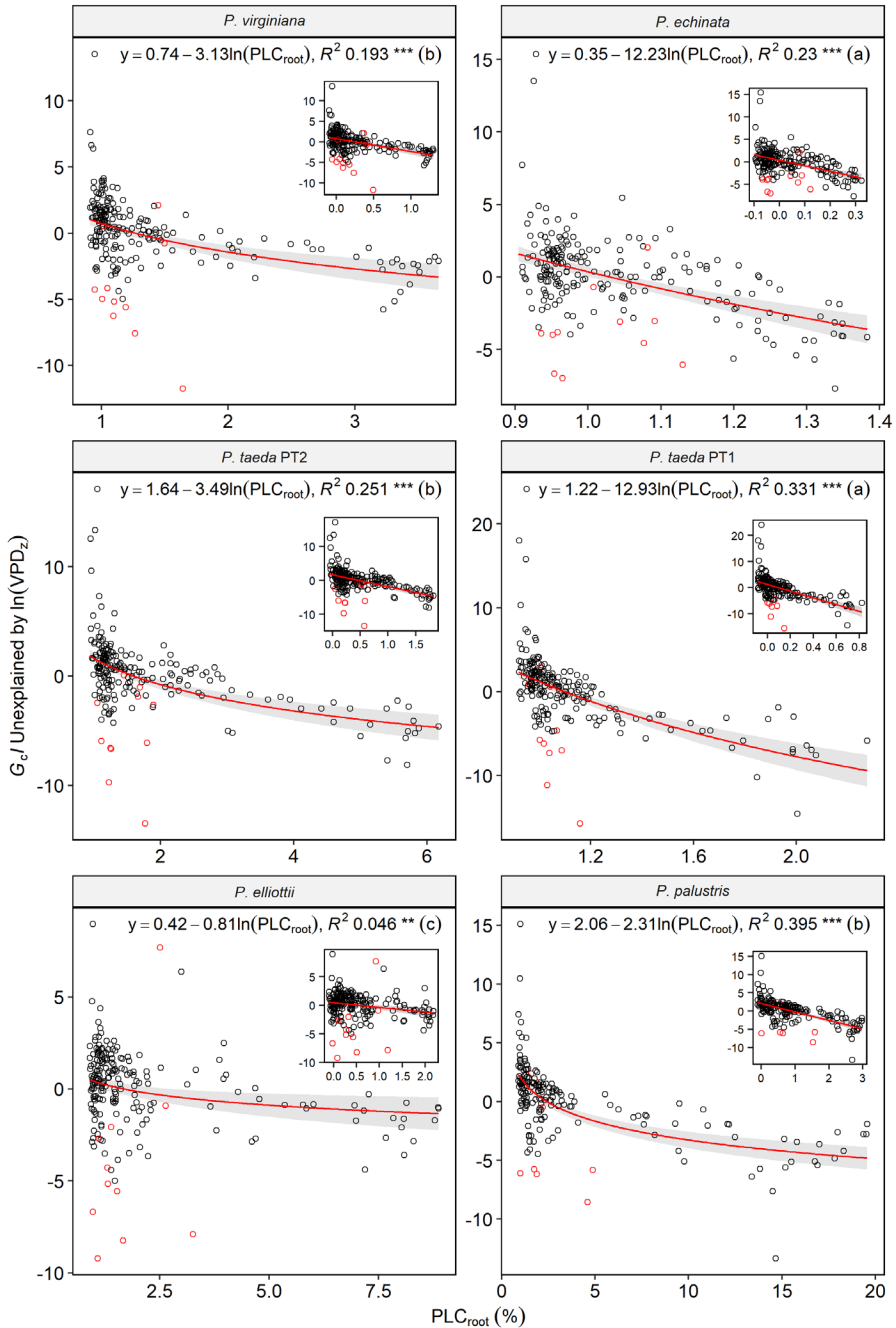


Fig S6. Regression of residual in canopy conductance index (G_cI) unexplained by normalized vapor pressure deficit (VPD_z) on the estimated *in situ* percent loss of conductivity in roots (PLC_{root}) using a linear-log relationship. PLC_{root} was derived from tree specific Ψ_s . Insets show regression and data points on the linear-log scale. P value: *** < 0.001 ; ** < 0.01 . Red points indicate occasions of plausible outliers for the regression and correspond to the red dashed lines in Fig 4, 5. Significance letters show results of Tukey test on the slope associated with $\ln(PLC_{root})$ using a full model that included species effect and interaction with the slope. Ribbons represent 95% confidence intervals.

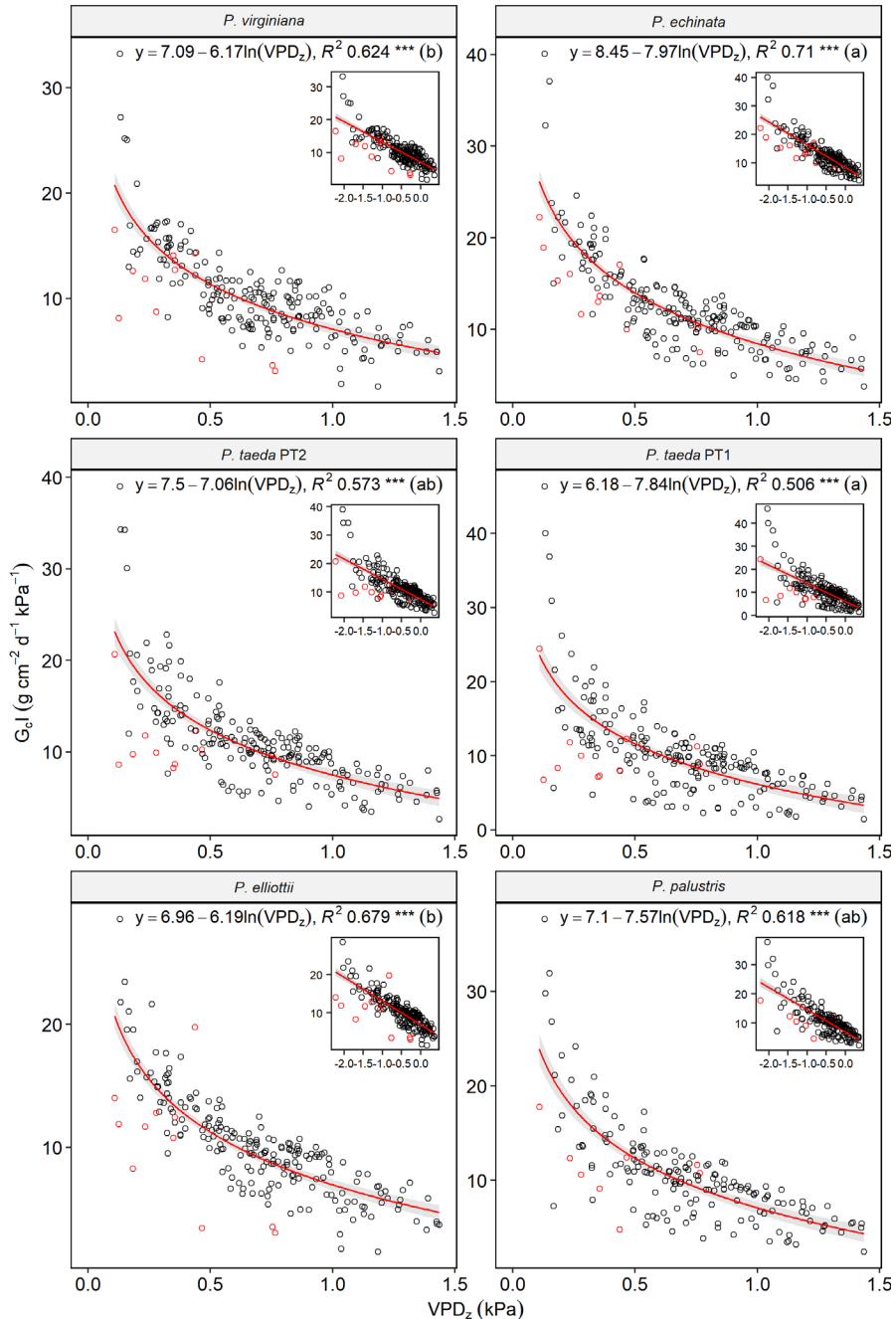


Fig S7. Regression of canopy conductance index (G_{cI}) on normalized vapor pressure deficit (VPD_z) using a linear-log relationship. Insets show regression and data points on the linear-log scale. P value: *** <0.001 . Red points indicate occasions of plausible outliers for the regression and correspond to the red dashed lines in Fig 4, 5. Significance letters show results of Tukey test on the slope associated with $\ln(\text{PLC}_{\text{root}})$ using a full model that included species effect and interaction with the slope. Ribbons represent 95% confidence intervals.